Relaxation and the Dynamics of Molecules in the Liquid Crystalline Phases

ARTICLE *in* PROGRESS IN NUCLEAR MAGNETIC RESONANCE SPECTROSCOPY · SEPTEMBER 2002

Impact Factor: 7.24 · DOI: 10.1016/S0079-6565(02)00037-7

1 AUTHOR:

Ronald Y Dong
University of British Columbia - Vancouver
219 PUBLICATIONS **2,261** CITATIONS

ELSEVIER

Progress in Nuclear Magnetic Resonance Spectroscopy 41 (2002) 115–151

PROGRESS IN NUCLEAR MAGNETIC RESONANCE SPECTROSCOPY

www.elsevier.com/locate/pnmrs

Relaxation and the dynamics of molecules in the liquid crystalline phases

Ronald Y. Dong[a,b,*]

[a]*Department of Physics and Astronomy, Brandon University, Brandon, Man., Canada R7A 6A9*
[b]*Department of Physics and Astronomy, University of Manitoba, Winnipeg, Man., Canada R3T 2N2*

Accepted 25 May 2002

Contents

Keywords: Liquid crystal; Anisotropy; Relaxation time

* Address: Department of Physics and Astronomy, Brandon University, Brandon, Man., Canada R7A 6A9. Tel.: +1-204-727-9695; fax: +1-204-728-7346.
E-mail address: dong@brandonu.ca (R.Y. Dong).

PII: S0079-6565(02)00037-7

Nomenclature

AFLC	anti-ferroelectric liquid crystal
AP	additive potential
BPP	Bloembergen, Purcell, Pound
cmc	critical micellar concentration
CS	chemical shielding
D	dipole–dipole
efg	electric field gradient
eQ	nuclear electric quadrupole moment
FLC	ferroelectric liquid crystal
JB	Jeener–Broekaert
L	laboratory frame
LC	liquid crystal
LCP	liquid crystalline polymer
M	molecular frame
MAS	magic angle spinning
MR	molecular rotations
ODF	order director fluctuations
PAS	principal axis system
PDLC	polymer dispersed liquid crystal
Q	quadrupolar
RIS	rotational isomeric state
RMTD	reorientation mediated by translational displacement
SD	self-diffusion
TR	translational diffusion mediated reorientations
N	nematic phase
RN	re-entrant nematic phase
SmA	smectic A phase
SmB	smectic B phase
SmC	smectic C phase
SmC*	chiral smectic C phase
uSmC*	unwound smectic C* phase
SmG	smectic G phase
T_1	spin–lattice relaxation time
T_{1D}	proton dipolar spin–lattice relaxation time
T_{1Q}	quadrupolar spin–lattice relaxation time
T_{1Z}	Zeeman spin–lattice relaxation time
T_2	spin–spin relaxation time

1. Introduction

Liquid crystalline materials can form anisotropic media either by varying the temperature or the concentration in certain solvents. The former is called thermotropic liquid crystals (LC), while the latter lyotropic LCs. The phenomenon of 'double melting' was discovered in several esters of cholesterol by Reinitzer [1] in 1888. These substances melt to an isotropic clear liquid only after an intermediate stable

phase in the form of an opaque liquid. Many fundamental advances in understanding LC phases were made before the mid 1960s. These included the model of long stiff rods by Onsager [2] which showed the role of repulsive forces, the Maier–Saupe statistical model [3] which pointed to the role of dispersion forces, and the model by Gelbart and Cotter [4,5] which united these two approaches in the Van der Waals theories. But the real push in LC research came only after the first realization of applying these materials in electro-optical technology [6]. Intense efforts in investigating many different physical properties of these materials, and in creating new and more stable materials through systematic synthetic work had began in late 1960s and continued up to the present. It is known that the molecular structure (e.g. shape anisotropy, calamitic versus discotic) has a strong influence on the phase structure of LCs. However, similar phase structures may occur in organic compounds of very different shapes. Some important mesomorphic phase structures in LCs are nematic, smectic, columnar and cubic (structure with micellar lattice units or complicated interwoven networks) phases. As a result of their shape anisotropy, molecules forming mesophases tend to align more or less about a spatial direction called the director, which is denoted by a unit vector $\hat{n}$. A quantitative measure of the parallelity of the molecules in mesophases is the (orientational) order parameter $S = 1/2\langle 3\cos^2\theta - 1\rangle$, where θ is the angle between $\hat{n}$ and the long axis of a molecule, and brackets denote the thermal average. The order parameter can be measured based on anisotropic properties of LCs. Experimental methods include optical measurements, magnetic properties, X-ray and nuclear magnetic resonance (NMR) investigations. In addition to the orientational ordering, positional order may also occur in layered structures shown by various kinds of smectic phases and lamellar phases. For molecules containing lateral electric dipole(s) and/or chiral center(s), the LC phases and subphases then process ferro- and/or antiferro-electric properties. The search for possible applications of newly discovered LC materials and phase structures is the primary reason for the continuing expansion of LC research. There are many excellent textbooks on the physics and chemistry of LCs [7–11], and the readers are asked to consult these materials for details of LCs.

Information about LC structures and dynamics can be obtained using NMR spectroscopy. Proton spin–lattice relaxation studies played a crucial role [12–16] in the late 1960s in identifying the unique collective dynamics known as order director fluctuations (ODF) in thermotropic LCs. Later, ODF involving two-dimensional or three-dimensional thermal excitations were found to be important in lipid bilayer dynamics [17]. Besides ODF, it was soon realized that LC molecules translationally diffuse and reorient as in normal liquids, although restrictions due to the phase structures must be taken into account. Furthermore, internal bond rotations also occur in LC molecules as their molecular structures usually are non-rigid. Typically, two kinds of NMR experiments are performed: one being a combination of high-field Zeeman order relaxation time (T_{1Z}) and high-field dipolar or quadrupolar order relaxation time (T_{1D} or T_{1Q}) experiments at a particular Larmor frequency $\omega_0/2\pi$ [18,19]; the other kind is frequency-dependent T_{1Z} and T_{1D} measurements over a broad range of Larmor frequencies using both conventional spectrometers and the field cycling technique [20,21]. These relaxation times can often be accounted for by means of superimposed molecular processes: collective ODF, and individual motions such as molecular rotations (MR) and translational self-diffusions (SD) as well as internal dynamics. Calculations of the second rank correlation functions and their Fourier transforms, the spectral densities of motion, are of interest in any nuclear spin relaxation theory. Various macroscopic relaxation observables can be related to the spectral densities arising from fluctuating second-rank spin couplings. Fitting the theoretical spectral densities, numerically or analytically, to experimental NMR relaxation rates and simulating lineshapes can be used to investigate the dynamics of LCs. Furthermore, the relations between molecular dynamics and macroscopic material properties are of interest to device applications of LCs.

In the Redfield limit [22], expressions for different spin relaxation rates can be derived using time-dependent perturbation theory. This approach is normally sufficient for treating spin relaxation in liquids and LCs, although in the slow motion regime the solution of the stochastic Liouville equation is required [23]. A slow-motional theory has recently been proposed to study the spin–spin relaxation due

to ODF by analytically solving the Liouville equation [24] through modeling the director fluctuations as a multidimensional Gaussian process. The present contribution is, however, limited to the Redfield theory in which the spin system is treated quantum-mechanically, while the lattice is treated semi-classically.

The article is organized as follows. Section 2 provides an overview of spin relaxation theory [25] in the context of LC studies. Section 3 outlines various models for different molecular processes: ODF, MR, SD and internal motions. Section 4 describes the current state of NMR relaxation studies in thermotropics with some attentions on the LC phase structures and viscoelastic properties. Section 5 briefly reviews the corresponding advances in lyotropics and biologically ordered fluids. Section 6 aims at some recent contributions of NMR in studying 'exotic' LC phases, and Section 7 provides some concluding remarks and outlook. Since the present article focuses on works reported in the literature over the past decade, we refer the reader to many existing books [26–29] for a more complete coverage of the literature.

2. Relaxation theory: an overview

The main formalism of nuclear spin relaxation was developed in the classical works by Bloembergen, Purcell and Pound [30], Wangsness and Bloch [31], Solomon [32], Bloch [33,34], Abragam [25], Redfield [22] and Tomita [35,36]. Here we adopt the fast motion (Redfield) limit for molecular systems in which the lattice can be treated classically and the spin–lattice coupling is treated as a random perturbation on the spin system. The spin–lattice coupling(s) can be of different kinds depending on the spin Hamiltonian of the spin system under consideration. These may include the magnetic dipole–dipole interaction, the nuclear quadrupole interaction, the spin–rotation interaction, the scalar coupling of the first and second kind, and the chemical shift anisotropy interaction. Due to the need to estimate the magnitude of certain nuclear couplings and/or correlation times associated with different types of motions, considerable uncertainty exists in identifying and separating these contributions. The coupling between the nuclear Zeeman reservoir and the lattice is magnetic in all cases (e.g. dipole–dipole interaction) except one. The exception is an electrical coupling between the nuclear electric quadrupole moment eQ and the lattice via an electric field gradient (efg). When the quadrupolar coupling exists, it is generally more efficient than any magnetic coupling. In this section, we survey the common nuclear spin Hamiltonians that occur in NMR studies of LCs, the density matrix formalism in connection to spectral densities of motion and the relevant NMR relaxation observables [25] from the spin relaxation theory.

2.1. Spin hamiltonian

In LCs, the main interest is in three types of spin interactions: dipole–dipole (D), electric quadrupole (Q) and chemical shielding (CS). All of these spin interactions may be formally written in terms of irreducible tensors of rank l [37]

$$H_\lambda = C_\lambda \sum_l \sum_{m=-l}^{l} (-1)^m T^\lambda_{l,m} R^\lambda_{l,-m} \tag{1}$$

where $l = 0$, 1 and 2 and the scalar factor C_λ is an appropriate constant for the spin interaction labeled by λ ($C_D = -\mu_0 \gamma_I \gamma_S \hbar^2/2\pi$, $C_Q = eQ/2I(2I-1)$ and $C_{CS} = \gamma_I \hbar$). The spin operators $T_{l,m}$ for $\lambda = D$ or Q in the laboratory (L) frame are

$$T_{0,0} = -\frac{1}{\sqrt{3}} \vec{I}\cdot\vec{S} \qquad T_{2,0} = \sqrt{\frac{1}{6}}(3I_Z S_Z - \vec{I}\cdot\vec{S})$$
$$T_{2,\pm 1} = \mp \frac{1}{2}(I_Z S_\pm + I_\pm S_Z) \qquad T_{2,\pm 2} = \frac{1}{2} I_\pm S_\pm . \tag{2}$$

For the heteronuclear dipole–dipole interaction, the spin $\vec{I} \neq \vec{S}$, whereas for homonuclear dipolar coupling or electric quadrupole coupling, $\vec{I} = \vec{S}$. For anisotropic chemical shielding, the spin operators are

$$T_{0,0} = -I_Z B_0/\sqrt{3}$$
$$T_{2,0} = \sqrt{2/3} I_Z B_0$$
$$T_{2,\pm 1} = \mp I_Z B_0/2$$
$$T_{2,\pm 2} = 0.$$

The coupling tensor $R_{l,m}$ in the laboratory frame is

time-dependent due to motions of spin-bearing molecules. It can be expressed in terms of the rotational transformation of the irreducible components $\rho_{l,n}$ in the principal axis system (PAS) to the laboratory frame by

$$R_{l,m} = \sum_n D^{l*}_{mn}(\Omega_{\mathrm{PL}})\rho_{l,n} \tag{3}$$

where $D^l_{m,n}(\Omega_{\mathrm{PL}})$ denotes the Wigner rotation matrices and Ω_{PL} denotes the Euler angles by which the laboratory frame is brought into coincidence with the PAS. Now

$$\rho_{2,0} = \sqrt{3/2}\Delta_\lambda$$

$$\rho_{2,\pm1} = 0$$

$$\rho_{2,\pm2} = \frac{1}{2}\Delta_\lambda\eta_\lambda$$

where Δ_λ and η_λ can be obtained from V_{ii}, the principal values of the coupling tensor V. For quadrupolar coupling, $\Delta_{\mathrm{Q}} = V_{ZZ} = eq$, the efg and $\eta_{\mathrm{Q}} = (V_{YY} - V_{XX})/V_{ZZ}$, the asymmetry parameter of the efg tensor, while for the dipolar case, $\eta_{\mathrm{D}} = 0$ and $\Delta_{\mathrm{D}} = \langle 1/r^3_{IS}\rangle$, where r_{IS} is the internuclear distance and brackets denote a vibrational average. For both the dipolar and quadrupolar cases, $\rho_{0,0} = 0$. For chemical shielding, $\rho_{0,0} = -(\sigma_{11} + \sigma_{22} + \sigma_{33})/\sqrt{2} = -(\mathrm{Tr}\,\sigma)/\sqrt{2}$, $\Delta_{\mathrm{CS}} = \sigma_{33} - 1/3\,\mathrm{Tr}\,\sigma$ and $\eta_{\mathrm{CS}} = (\sigma_{22} - \sigma_{11})/\sigma_{33}$, where $\sigma_{\alpha\beta}$ are the chemical shielding tensor elements. For other spin couplings like spin–rotation and indirect spin–spin coupling (j-coupling), Eq. (1) still applies [37].

2.2. Evolution of density matrix

We consider a nuclear spin system whose Hamiltonian consists of a time-independent Hamiltonian H_0 and a small spin–lattice coupling $H_\lambda(t)$ of non-zero average value

$$H = H_0 + H_\lambda(t). \tag{4}$$

The spin–lattice Hamiltonian $H_\lambda(t)$ is taken as a stationary random function. It is convenient to consider the evolution of the density matrix ρ in the interaction picture by removing the static Hamiltonian H_0 (i.e. Zeeman interaction)

$$\frac{\partial\tilde{\rho}}{\partial t} = -\mathrm{i}[\tilde{H}_\lambda(t) - \langle\tilde{H}_\lambda(t)\rangle, \tilde{\rho}] \tag{5}$$

where the tilde represents the corresponding operator in the interaction representation, the angular brackets denote the time averaging, and the square brackets denote the commutator [25,38]. The Hamiltonian $\tilde{H}_\lambda(t)$ has double time dependencies, one from its random character and the other from going to the interaction representation

$$\tilde{H}_\lambda(t) = \exp(\mathrm{i}H_0t)H_\lambda(t)\exp(-\mathrm{i}H_0t). \tag{6}$$

The solution of Eq. (5) is obtained by a formal integration

$$\tilde{\rho}(t) = \tilde{\rho}(0) - \mathrm{i}\int_0^t [\tilde{H}_\lambda(t') - \langle\tilde{H}_\lambda(t')\rangle, \tilde{\rho}(t')]\mathrm{d}t'. \tag{7}$$

Substituting Eq. (7) into Eq. (5), and neglecting the correlation between the density matrix and the fluctuating spin–lattice coupling, one obtains to first order

$$\frac{\partial\tilde{\rho}(t)}{\partial t} = -\int_0^\infty \langle[\tilde{H}_\lambda(t) - \langle\tilde{H}_\lambda\rangle, [\tilde{H}_\lambda(t-\tau) - \langle\tilde{H}_\lambda\rangle, \tilde{\rho}(t) - \tilde{\rho}_{\mathrm{eq}}]]\rangle\mathrm{d}\tau \tag{8}$$

where $\tilde{\rho}(t)$ on the right side of the above equation has been replaced by $\tilde{\rho}(t) - \tilde{\rho}_{\mathrm{eq}}$ with $\tilde{\rho}_{\mathrm{eq}}$ being the thermal equilibrium value of the density matrix for the static Hamiltonian H_0, and the angular brackets over the double commutators denote an ensemble average. Let us consider H_λ in Eq. (1) with rank $l = 2$ only. In the interaction representation, it can be shown that [25]

$$\tilde{T}_{2,m}(t) = \sum_q T^{(2)}_{m,q}\,\mathrm{e}^{-\mathrm{i}\omega_{m,q}t} \tag{9}$$

where $\omega_{m,q}$ are the characteristic frequencies arising through transforming to the interaction picture and can be expressed in terms of a linear combination of the resonant frequencies of the relaxing spin(s). It is clear that in the laboratory (L) frame, $T_{2,m}$ is time-independent and given by $\sum_q T^{(2)}_{m,q}$. Using Eqs. (1), (6) in Eq. (8) and the fact that $H_\lambda(t)$ is Hermitian, one

obtains [25]

$$\frac{\partial\tilde{\rho}(t)}{\partial t} = -(C_\lambda\rho_{2,0})^2\sum_{m,q}\int_0^\infty G_m(\tau)\mathrm{e}^{-\mathrm{i}\omega_{m,q}\tau} \times\Big[T^2_{m,q},\Big[T^2_{-m,q},\tilde{\rho}(t)-\tilde{\rho}_{\mathrm{eq}}\Big]\Big]\mathrm{d}\tau \tag{10}$$

where the correlation functions $G_m(\tau)$

$$G_m(\tau) = \Big\langle\Big(R^*_{2,m}(t+\tau)-\Big\langle R^*_{2,m}\Big\rangle\Big)(R_{2,m}(t)-\langle R_{2,m}\rangle)\Big\rangle/(\rho_{2,0})^2 \tag{11}$$

describe the dynamics of a unique interaction component Δ_λ. For the special case of $\eta_\lambda = 0$, $R_{2,-m} = (-1)^m D^2_{m0}(\Omega_{\mathrm{PL}})\rho_{2,0}$ and $G_m(\tau)$ reduces to

$$G_m(\tau) = \Big\langle\Big(D^{2*}_{m0}(\Omega_{\mathrm{PL}},t+\tau) -\Big\langle D^{2*}_{m0}\Big\rangle\Big)\Big(D^2_{m0}(\Omega_{\mathrm{PL},}t)-\Big\langle D^2_{m0}\Big\rangle\Big)\Big\rangle. \tag{12}$$

Finally, using the irreducible spectral density of motion $J_m(\omega_{m,q})$ as the Fourier transforms of $G_m(\tau)$, one can rewrite Eq. (10) as

$$\frac{\partial\tilde{\rho}(t)}{\partial t} = -(C_\lambda\rho_{2,0})^2\sum_m\sum_q J_m(\omega_{m,q}) \times\Big[T^{(2)}_{m,q},\Big[T^{(2)}_{m,q},\tilde{\rho}(t)-\tilde{\rho}_{\mathrm{eq}}\Big]\Big] \tag{13}$$

where

$$J_m(\omega_{m,q}) = \int_0^\infty G_m(\tau)\mathrm{e}^{-\mathrm{i}\omega_{m,q}\tau}\,\mathrm{d}\tau. \tag{14}$$

Now Eq. (13) can be used to evaluate any observable operator A since the expectation (mean) value $\langle A\rangle = \mathrm{Tr}(\rho A)$. For instance, A can be one of the relaxation observables for a spin system. Thus, the relaxation rate can be written as a linear combination of irreducible spectral densities and the coefficients of expansion are obtained by evaluating the double commutators for a specific spin–lattice interaction λ. In working out $G_m(\tau)$ (e.g. Eq. (12)), one can use successive transformations from the PAS to the laboratory frame and the closure property of the rotation group to rewrite $D^2_{m0}(\Omega_{\mathrm{PL}})$ so as to include the effects of local segmental, molecular, and/or collective motions for molecules in LCs. The calculated irreducible spectral densities, therefore, contain all the frequency and orientational information pertaining to the studied molecular system.

2.3. Relaxation rates

The spin relaxation rates at different Larmor frequencies probe the power spectrum (i.e. Fourier intensities) of molecular motions. This is due to the fact that magnetic dipole transitions between the energy levels of a spin system in a magnetic field are possible only if the transition energy matches the energy quantum of the motional spectrum. In addition, relaxation rates for various spin–lattice interactions must be worked out in terms of spectral densities of motion based on Eq. (13) [19,25,39]. Here we collect some well known expressions of spin relaxation rates for common nuclei such as ^{1}H, ^{2}H, ^{14}N and ^{13}C used in LC studies.

2.3.1. Quadrupolar relaxation ($I = 1$)

The spin–lattice relaxation rate of the Zeeman order, i.e. $\langle I_Z\rangle$ and of the quadrupolar order, i.e. $\langle 3I^2_Z - 2\rangle$, can be shown to follow respective expressions in terms of $J_m(m\omega)$

$$T^{-1}_{1Z} = K_Q[J_1(\omega_0) + 4J_2(2\omega_0)] \tag{15}$$

$$T^{-1}_{1Q} = K_Q[3J_1(\omega_0)] \tag{16}$$

where $K_Q = (3\pi^2/2)(e^2qQ/h)^2$ with e^2qQ/h being the quadrupolar coupling constant, and the asymmetry parameter η for the quadrupolar coupling is assumed to be zero. For deuteron or nitrogen-14, there are three spin eigenstates $|1\rangle$, $|0\rangle$ and $|-1\rangle$ for the static Hamiltonian, whose corresponding populations are P_1, P_0 and P_{-1}. While the Zeeman order is given by the population difference $P_1 - P_{-1}$, the quadrupolar order involves a linear combination of all populations $2P_0 - P_1 - P_{-1}$. The T_{1Z} and T_{1Q} can be simultaneously measured using the Jeener–Broekaert (JB) pulse sequence $90°_x-\tau-45°_y-\tau-45°_y$ [19,40] or its broadband version given by the Wimperis sequence [41,42]. It is noted that the secular ($m = 0$) spectral density, which contains information about molecular motions on all time scales (within the motional narrowing limit), is not involved in T_1, the spin–lattice relaxation time. The non-secular ($m = 1, 2$) spectral densities are affected by motions on a time scale faster than the reciprocal Larmor frequency

(typically $< 10^{-7}$ s). To investigate slow motions, one can do field cycling experiments in order to lower the Larmor frequency, or measure the spin–spin relaxation rates. For the deuteron, three independent spin–spin relaxation times can be measured [43,44].

$$T_{2a}^{-1} = K_Q\Big[\tfrac{3}{2}J_0(0) + \tfrac{5}{2}J_1(\omega_0) + J_2(2\omega_0)\Big] \quad (17)$$

$$T_{2b}^{-1} = K_Q\Big[\tfrac{3}{2}J_0(0) + \tfrac{1}{2}J_1(\omega_0) + J_2(2\omega_0)\Big] \quad (18)$$

$$T_{2D}^{-1} = K_Q[J_1(\omega_0) + 2J_2(2\omega_0)]. \quad (19)$$

The spin–spin relaxation time T_{2a} can be measured by a quadrupolar echo pulse train $90°_x-\tau-90°_y-(2\tau-90°_y)_n$ if the pulse spacing $\tau \ll 2/\Delta\nu$ is satisfied (i.e. the deuteron spin relaxes as if the quadrupolar splitting $\Delta\nu$ is absent or a non-selective excitation is achieved). Due to the large quadrupolar splitting often encountered in LCs, the above condition for τ cannot be achieved experimentally and the two lines relax independently (i.e. $\tau > 2/\Delta\nu$ or selective excitation of half of the doublet exists). The quadrupolar echo pulse train then measures [45]

$$T_2^{-1} = K_Q\Big[\tfrac{3}{2}J_0(0) + \tfrac{3}{2}J_1(\omega_0) + J_2(2\omega_0)\Big] \quad (20)$$

instead. Finally, the double quantum (2D) spin–spin relaxation time T_{2D} can be determined using a 2D spin echo pulse sequence $90°_x-\tau-90°_x-t_1/2-180°-t_1/2-90°$. The first two 90° pulses create the 2D coherence, which is refocused by a 180° pulse and the spin echo is detected by the last 90° pulse.

2.3.2. Dipole–dipole relaxation

Here we have to distinguish between homonuclear and heteronuclear (unlike) spin-1/2 pairs. The latter gives rise to the so-called 3/2 effect [25]. For an isolated pair of like spin-1/2 nuclei ($I = 1$) separated by an internuclear distance r, the treatment of spin relaxation is identical to that for a spin-1 quadrupole system. The Zeeman spin–lattice relaxation time T_{1Z} and spin–spin relaxation time T_2 are given, respectively, by Eqs. (15), (17) except the interaction parameter K_Q is now replaced by the corresponding factor in the SI units $K_D = (3/2)(\mu_0\gamma^2\hbar/4\pi r^3)^2$, i.e.

$$T_{1Z}^{-1} = K_D[J_1(\omega_0) + 4J_2(2\omega_0)] \quad (21)$$

$$T_2^{-1} = K_D\Big[\tfrac{3}{2}J_0(0) + \tfrac{5}{2}J_1(\omega_0) + J_2(2\omega_0)\Big]. \quad (22)$$

The dipolar spin–lattice relaxation time T_{1D} is for relaxing the dipolar order to the lattice, and can be determined using the Jeener–Broekaert sequence. In LCs, the proton system may be considered as an ensemble of isolated spin pairs. This is based on the fact that neighboring molecules have relatively fast diffusive motions which average out the intermolecular dipolar interactions. In this limit and using the high spin–temperature approximation [25]

$$T_{1D}^{-1} = K_D[3J_1(\omega_0)_{intra}] \quad (23)$$

where the subscript intra in $J_1(\omega_0)$ is to emphasize the contribution from an isolated spin-1/2 pair within a molecule (and only the first nearest neighboring spin yields the major contribution). Eq. (23) is similar to T_{1Q}^{-1} given by Eq. (16). Skepticism remains on the validity of Eq. (23), as the prediction of $T_{1Z}/T_{1D} = 3$ in the limit of $J_2(2\omega_0)$ being negligible is seldom observed in proton relaxation experiments on LCs. Thus, possible contributions to T_{1D} from multispin interactions and correlations have been examined [46], but found to be negligible. Eq. (23) has recently been modified by removing the short correlation time approximation, i.e. the secular dipolar Hamiltonian is now included with the Zeeman Hamiltonian to work out the time dependence of the spin operators in the Redfield high temperature theory [47]. The complex problem of spin correlations and dipolar relaxation without the high spin–temperature approximation has also been addressed, i.e. including second (and higher) order in ω/kT [48].

For heteronuclear dipolar relaxation, we consider dipole–dipole couplings between two unlike spin-1/2 nuclei I and S (e.g. ^{13}C–H pair). The Zeeman spin–lattice (T_1) and spin–spin (T_2) relaxation times for the I spin are given, respectively, by

$$T_{1Z}^{-1} = K'_D\Big[\tfrac{1}{3}J_0(\omega_I - \omega_S) + J_1(\omega_I) + 2J_2(\omega_I + \omega_S)\Big] \quad (24)$$

$$T_2^{-1} = K'_D\Big[\tfrac{2}{3}J_0(0) + \tfrac{1}{6}J_0(\omega_I - \omega_S) + \tfrac{1}{2}J_1(\omega_I) + J_1(\omega_S) + J_2(\omega_I + \omega_S)\Big] \quad (25)$$

where $K'_D = (3/2)(\mu_0\gamma_I\gamma_S\hbar/4\pi r_{IS}^3)^2$.

2.3.3. Chemical shielding anisotropy relaxation

The magnetic field at a resonant nucleus depends

on the applied external B_0 field, as well as the screening of the applied field at the nucleus by the surrounding electrons. As the shielding (or chemical shift) tensor σ is anisotropic, the principal component σ_{ZZ} fluctuates with time as a result of modulations by molecular motions. Taking into account the asymmetry parameter η of the shielding tensor ($\eta = (\sigma_{XX} - \sigma_{YY})/\sigma_{ZZ}$), the Zeeman spin–lattice (T_1) and spin–spin (T_2) relaxation times due to shielding anisotropy are given, respectively, by [25]

$$T_{1Z}^{-1} = \tfrac{3}{2}(\gamma B_0 \sigma_{ZZ})^2 \left(1 + \frac{\eta^2}{3}\right) J_1(\omega_0)$$

$$T_2^{-1} = (\gamma B_0 \sigma_{ZZ})^2 \left(1 + \frac{\eta^2}{3}\right) \left[J_0(0) + \tfrac{3}{4} J_1(\omega_0) \right]. \quad (26)$$

The relaxation rates due to chemical shielding anisotropy depend on the square of the applied B_0 field. Hence the chemical shielding tends to dominate at high fields and for nuclei exhibiting large chemical shifts. It is noted that the above spin–lattice and spin–spin relaxation rates do not coincide in the motional narrowing limit.

2.3.4. Angular-dependent relaxation

The orientational information in the irreducible spectral densities (see Eq. (14)) comes from the Wigner rotation matrices $D^2_{m0}(\Omega_{\mathrm{PL}})$. In LCs, it is customary to write the irreducible spectral densities given in the laboratory frame in terms of spectral densities expressed in the crystal-frame, which is defined by the symmetry axis (director) of the phase. In the case of the director not aligned along the external magnetic field, the extra transformation involving Euler angle $\Omega_{\mathrm{LD}}(\equiv \phi_{\mathrm{LD}}, \theta_{\mathrm{LD}})$ from the crystal-frame to the L frame produces certain linear combination of the crystal-frame spectral densities $J^{\mathrm{C}}_{np}(\omega_m)$ according to [49–52]

$$J_m(\omega_m; \Omega_{\mathrm{LD}}) = \sum_{n,p} d^2_{mn}(\theta_{\mathrm{LD}}) d^2_{mp}(\theta_{\mathrm{LD}}) \times \exp[\mathrm{i}(n-p)\phi_{\mathrm{LD}}] J^{\mathrm{C}}_{np}(\omega_m) \quad (27)$$

where $m = 0,\ 1{,}2,\ \omega_m = m\omega_0$ for quadrupolar or homonuclear dipolar couplings, and $\omega_m = \omega_I + (m-1)\omega_S$ for heteronuclear dipolar couplings. The crystal-frame spectral densities $J^{\mathrm{C}}_{np}(\omega_m)$ depend on the intrinsic properties (e.g. phase symmetry) of LCs. For instance, in uniaxial mesophases ($n = p$) the crystal-frame spectral densities revert to the irreducible spectral densities without the angular information when $\Omega_{\mathrm{LD}} = 0$, and $J^{\mathrm{C}}_{mm}(\omega_m) = J_m(\omega_m)$ (for simplicity, the superscript C has been dropped hereafter). Writing out Eq. (27) for the three irreducible spectral densities, one obtains in biaxial liquid crystalline phases [50]

$$\begin{aligned} J_0(0;\Omega) = {} & \tfrac{1}{4}(3\cos^2\theta - 1)^2 J_{00}(0) \\ & + 3\cos^2\theta \sin^2\theta J_{11}(0) + \tfrac{3}{4}\sin^4\theta J_{22}(0) \\ & + radic; 6\cos 2\phi \sin^2\theta J_{20}(0) \\ & - \tfrac{3}{4}\cos 2\phi \sin 2\theta J_{1-1}(0) \\ & - \tfrac{3}{4}\cos 4\phi \sin^2\theta J_{2-2}(0) \end{aligned} \quad (28)$$

$$\begin{aligned} J_1(\omega;\Omega) = {} & \tfrac{3}{2}\sin^2\theta\cos^2\theta J_{00}(\omega) + \tfrac{1}{2}(1 - 3\cos^2\theta \\ & + 4\cos^4\theta) J_{11}(\omega) + \tfrac{1}{2}(1 - \cos^4\theta) J_{22}(\omega) \\ & - radic; 6\cos 2\phi \sin^2\theta \cos^2\theta J_{20}(\omega) \\ & - \tfrac{1}{2}\cos 2\phi (1 - 5\cos^2\theta \\ & + 4\cos^4\theta) J_{1-1}(\omega) \\ & - \tfrac{1}{2}\cos 4\phi (1 - \cos^2\theta)^2 J_{2-2}(\omega) \end{aligned} \quad (29)$$

$$\begin{aligned} J_2(2\omega;\Omega) = {} & \tfrac{3}{8}(1 - \cos^2\theta)^2 J_{00}(2\omega) \\ & + \tfrac{1}{2}(1 - \cos^4\theta) J_{11}(2\omega) \\ & + \tfrac{1}{8}(1 + 6\cos^2\theta + \cos^4\theta) J_{22}(2\omega) \\ & + \tfrac{\sqrt{6}}{4}\cos 2\phi (1 - \cos^4\theta) J_{20}(2\omega) \\ & + \tfrac{1}{2}\cos 2\phi (1 - \cos^2\theta)^2 J_{1-1}(2\omega) \\ & + \tfrac{1}{8}\cos 4\phi (1 - \cos^2\theta)^2 J_{2-2}(2\omega) \end{aligned} \quad (30)$$

where $J_{20}(\omega)$, $J_{1-1}(\omega)$ and $J_{2-2}(\omega)$ are only non-zero in biaxial phases. Thus, Eqs. (28)–(30) reduce to the familiar expressions in uniaxial phases [19]. It is

noted that even in biaxial mesophases, the biaxial spectral densities are unobservable if the director is aligned with the applied magnetic field as in some smectic C (SmC) phases. Biaxial spectral densities due to molecular reorientations in biaxial phases have been theoretically calculated based on the small step rotational diffusion model [51,52]. Thus far, no experiments have been reported on the determination of biaxial spectral densities.

3. Dynamical processes: motional models

The crystal-frame spectral densities may be obtained experimentally without resorting to any motional model, i.e. they are model-free spectral parameters obtained from spin relaxation measurements. To connect them to the physical systems in terms of their macroscopic properties, one needs to turn to the mathematical description of various motional models. In LCs, several dynamical processes are known to simultaneously influence the nuclear spin relaxation. To achieve a composite model for all the relevant motional processes is a daunting task, especially when the time scales of the motional processes become comparable, thereby producing coupling effects among them. In practice, time scale arguments are often used to simplify the complexity of the model. However, there is no unique way to carry out different levels of approximations, and the composite models used by different authors simply reflect the preference and philosophy of the author. In general, different molecular dynamics in LCs can be grouped into non-collective (individual) and collective motions. The non-collective motions include individual MRs and translational SDs. There appears a general consensus in the LC community that molecular reorientation under the influence of a potential of mean torque set up by the neighbours can be described by the small step rotational diffusion model [51–58] with various levels of refinements. The problem of roto-translational diffusion for molecules reorienting in uniaxial smectic phases has also been considered [59,60] theoretically. This theory has yet to be tested by NMR relaxation experiments. Translational SDs can be important when proton spin relaxation is used to study LCs. This is due to modulations of inter-proton distances between two diffusing molecules. SD may also enter indirectly in the treatment of relaxation due to ODFs. Spin relaxation by translational diffusions is formulated [25] by solving a translational diffusion equation. Theories for SD in isotropic liquids and cubic solids [61–64] have been extended to LCs in the nematic (N) [65], smectic A (SmA) [66] and smectic B (SmB) [67] phases.

The constituent molecules of LCs invariably compose of flexible chain(s) and a 'rigid' molecular core. In addition to the overall motion of the molecule, internal bond rotations within the flexible chain must also be taken into account. These conformational transitions are much faster than the rotational diffusive motion of the molecular core. There are different approaches to incorporate the internal rotations in LC molecules: segmental diffusion model [68,69], superimposed rotations model [70] and the decoupled model [71–73]. In studying lipid bilayers of membrane systems, Brown and co-workers have utilized the segmental diffusion model in which local segmental motions are taken first to give a motionally averaged quadrupolar coupling in an intermediate frame for each deuteron along the lipid acyl chain. The intermediate frame at each carbon site is chosen so that the residual quadrupolar coupling tensor is diagonal and specified by two unknown model parameters χ_Q^{eff} and η_Q^{eff}. Here η_Q^{eff} is a motional-induced asymmetry parameter for the quadrupolar interaction. In addition, the Euler angles for the transformation from each intermediate frame to the molecular frame (for example, defined by the principal frame of the rotation diffusion tensor for the lipid molecule) are time-independent and are also treated as model parameters. In practice, this particular approach can involve up to three adjustable parameters in order to model the internal dynamics at each carbon site along the acyl chain. The segmental diffusion model differs from the superimposed rotations model and the decoupled model, because the latter models rely on a crucial assumption that the rotational diffusive motion of the entire molecule is independent of the fast conformational changes, which occur in the flexible chain. In the superimposed rotations model, the carbon–carbon bonds in the chain are assumed to rotate freely (i.e. free rotational diffusion) and independent of each other. For each C_i-C_{i+1} bond, the superimposed

rotations model must introduce an additional correlation time τ_i to account for its rotation with respect to its previous bond in the chain. The predictions of this model are consistent with the experimental observations that the deuteron spin–lattice relaxation rates $R^{(i)}$ decrease monotonically along the chain [70,74–77] in LCs. The same trend has also been observed in ^{13}C spin–lattice relaxation rates [78,79]. However, the presence of the potential of mean torque in LCs has made the assumption of independent bond rotations questionable. Later, correlated internal motions are considered explicitly by generating all possible conformations for a LC molecule using Flory's isomeric model [80]. These conformations are weighted by their equilibrium probabilities which are calculated by assuming a form for the potential of mean torque. This approach leads to the decoupled model proposed independently by us [71,72] and Nordio [73].

3.1. Order director fluctuations

Thermal excitations of the orientation of the director involve collective motions of a large number of molecules in an anisotropic elastic continuum. ODF can be either two-dimensional excitations observed in smectic and lamellar phases [81,82] or three-dimensional excitations in nematics [83,84], and they show quite different frequency dependences. NMR field cycling experiments are instrumental in demonstrating that the ODF mechanism can dominate the spin–lattice relaxation dispersion at Larmor frequencies below 1 MHz [85]. Here we summarize the results of spectral density calculations for the ODF mechanism [27].

It is well known that by using a small angle (θ) approximation, where θ is the angle between the instantaneous director and its equilibrium orientation, ODF contribute to $J_1(\omega)$ only. When taking high-order terms of $\theta\,(\propto\theta^2)$ in the case where θ is not small, contributions from ODF to $J_0(\omega)$ and $J_2(2\omega)$ become non-zero. Indeed, there is a small correction to $J_1(\omega)$ due to the second-order contribution. Because ODF involve a distribution of correlation times or long wavelength modes, the spectral densities show characteristic frequency behaviors. Two aspects of the ODF spectral density will be highlighted here: (1) chain flexibility, and (2) orientation dependence of the equilibrium director with respect to the external B_0 field. When the principal component of the spin interaction (e.g. C–D bond) is fixed with respect to an assumed axis of cylindrical symmetry of the molecule given by the angle $\beta_{M,Q}$, the spectral densities are given to second-order in θ for nematics by [84,86,87]

$$J_0(\omega) = A^2 \frac{\langle P_2\rangle^2}{(1-3\alpha)^2}\left[d^2_{00}(\beta_{M,Q})\right]^2 \frac{1}{\pi}\ln\left[1+\left(\frac{\omega_c}{\omega}\right)^2\right] \tag{31}$$

$$J_1(\omega) = A\frac{\langle P_2\rangle^2}{(1-3\alpha)^2}\left[d^2_{00}(\beta_{M,Q})\right]^2 \times(1-4\alpha)U\left(\frac{\omega_c}{\omega}\right)\omega^{-1/2} \tag{32}$$

$$J_2(2\omega) = A^2\frac{\langle P_2\rangle^2}{(1-3\alpha)^2}\left[d^2_{00}(\beta_{M,Q})\right]^2 \frac{1}{3\pi} \times\ln\left[1+\left(\frac{\omega_c}{2\omega}\right)^2\right] \tag{33}$$

where $\langle P_2\rangle$ is the nematic order parameter, the cutoff function $U(\omega_c/\omega)$ accounts for the cutoff of coherence modes at high frequencies

$$U(x) = \frac{1}{2\pi}\ln\left[\frac{x-\sqrt{2x}+1}{x+\sqrt{2x}+1}\right] + \frac{1}{\pi}[\tan^{-1}(\sqrt{2x}-1) + \tan^{-1}(\sqrt{2x}+1)], \tag{34}$$

the prefactor A is given by

$$A = \frac{3kT}{4\sqrt{2}\pi}\left(\frac{\eta}{K^3}\right)^{1/2} = \frac{3\pi\alpha}{2\sqrt{2\omega_c}} \tag{35}$$

ω_c is the high frequency cutoff, K is the average elastic constant, η is the average viscosity and the parameter α, defined by Eq. (35) is a measure of the magnitude of director fluctuations ($\alpha \ll 1$). For C–D bonds located in the flexible chain, the effect of ODF is made smaller as a result of additional averaging of the time-dependent factor $d^2_{00}(\beta_{M,Q})$ by conformational transitions in the chain. Taking this into account, the spectral densities in Eqs. (31)–(33) can still be used if $\langle P_2\rangle d^2_{00}(\beta_{M,Q})$ is replaced by the segmental order parameter S_{CD} of the C–D bond at a particular carbon site on the chain [88,89]. Thus, when ODF dominate the relaxation rates the spectral densities in a flexible

chain show a S^2_{CD} dependence as observed experimentally [90,91]. When the equilibrium director is oriented at an angle θ_{LD} with respect to the external magnetic field, the general expression for $J_m(\omega;\theta_{LD})$ in uniaxial LC phases due to ODF is given according to Eq. (27)

$$J_m(\omega;\theta_{LD}) = \frac{3\pi}{8}\frac{S^2_{CD}}{(1-3\alpha)^2}\left\{\frac{3\alpha^2}{\omega_c}\ln(1+x^2)\times\left[d^2_{m0}(\theta_{LD})\right]^2+\frac{4\alpha}{\sqrt{2\omega_c}}\frac{(1-4\alpha)}{\sqrt{\omega}}U(x)\times\left(\left[d^2_{m1}(\theta_{LD})\right]^2+\left[d^2_{m-1}(\theta_{LD})\right]^2\right)+\frac{\alpha^2}{\omega_c}\ln(1+x^2)\left(\left[d^2_{m2}(\theta_{LD})\right]^2+\left[d^2_{m-2}(\theta_{LD})\right]^2\right)\right\} \quad (36)$$

where $x = \omega_c/\omega$.

In SmA and lamellar phases, all twist modes are forbidden due to the relatively large values of twist elastic constant (K_2), resulting in a different frequency dependence for two-dimensional ODF. Thus, the spectral density $J_1(\omega)$ for two-dimensional director fluctuations (or layer undulations) is given by [82]

$$J_1(\omega) = \frac{3}{4}\left(\frac{kT}{2K}\right)\frac{S^2_{CD}}{(1-3\alpha)^2}\omega^{-1}. \quad (37)$$

It is worthwhile to point out that a recent molecular dynamics simulation of the hydrocarbon chain in lipid bilayers [92] has indicated that the chain isomerization shows a power law relaxation in the time domain and an associated $\omega^{-1/2}$ frequency dependence without the need of director fluctuations.

3.2. Molecular diffusion models

MRs can be treated as small step angular diffusion in the presence of a potential of mean torque [51–54,93]. To calculate the correlation functions for molecular reorientations, the rotational diffusion equation must be solved to give the conditional probability for a rigid molecule in a certain orientation at time t given that it has a different orientation at $t = 0$ and the equilibrium probability for finding the molecule with a certain orientation. It is well known that these orientation correlation functions can be written as a sum of decaying exponentials [54]. In the notation of Tarroni and Zannoni [57], one obtains for a reorienting symmetric top molecule

$$g^R_{mn}(t) = \sum_k \left(A^2_{mn}\right)_k \exp\left[\left(B^2_{mn}\right)_k t\right] \quad (38)$$

where m and n represent the projection indices of a rank 2 tensor in the L and M frames, respectively, $(B^2_{mn})_k/D_\perp$, the decay constants, are the eigenvalues of the rotational diffusion matrix and $(A^2_{mn})_k$, the relative weights of the exponentials, are the corresponding eigenvectors. In this model, the rotational diffusion tensor is diagonalized in a molecular frame with principal components $D_\parallel$ and $D_\perp$. These rotational diffusion constants enter into the decay constants. $D_\parallel$ and $D_\perp$ specify the molecular reorientation about the molecular long axis (the axis of assumed cylindrical symmetry) and of the short axis, respectively. The spectral densities for a deuteron residing on the rigid part of a molecule are given by

$$J^R_m(m\omega) = \sum_n \left[d^2_{n0}(\beta_{M,Q})\right]^2 \sum_k \frac{(A^2_{mn})_k + (B^2_{mn})_k}{(m\omega)^2 + (B^2_{mn})_k} \quad (39)$$

where $m = 0, 1, 2$. Numerical solutions for cylindrical molecules reorienting in uniaxial phases have been provided by Vold and Vold [56] using only three leading terms in Eq. (38), viz.

$$g^R_{mn}(t) = c_{mn}\sum_{j=1}^{3} a^{(j)}_{mn}\exp\left[-t/\tau^{(j)}_{mn}\right] \quad (40)$$

where c_{mn}, the mean square average of the Wigner rotation matrices, are the initial amplitudes of the correlation functions

$$c_{mn} = \left\langle \left| D^2_{mn}(\Omega)\right|^2\right\rangle - \left(\overline{D^2_{00}}\right)^2 \quad (41)$$

$a^{(j)}_{mn}$ represent the normalized weight of each exponential whose time constant is

$$\left[\tau^{(j)}_{mn}\right]^{-1} = \frac{6D_\perp}{b^{(j)}_{mn}} + n^2(D_\parallel - D_\perp). \quad (42)$$

The $a^{(j)}_{mn}$, $b^{(j)}_{mn}$ and c_{mn} coefficients for all the correlation functions are given numerically as polynomials in $\langle P_2\rangle$ and their expansion coefficients are tabulated in Table 1 of Ref. [56] for a Maier–Saupe potential. The corresponding spectral densities are

given by

$$J_m^{\mathrm{R}}(m\omega) = \sum_n \left[d_{n0}^2(\beta_{\mathrm{M,Q}})\right]^2 c_{mn} \sum_j \frac{a_{mn}^{(j)}\left(\tau_{mn}^{(j)}\right)^{-1}}{(m\omega)^2 + \left(\tau_{mn}^{(j)}\right)^{-2}}. \tag{43}$$

In the single exponential approximation for $g_{mn}^{\mathrm{R}}(t)$ [53], the spectral densities simply to

$$J_m^{\mathrm{R}}(m\omega) = \sum_n \left[d_{n0}^2(\beta_{\mathrm{M,Q}})\right]^2 c_{mn} \frac{a_{mn}(\tau_{mn})^{-1}}{(m\omega)^2 + (\tau_{mn})^{-2}} \tag{44}$$

where the superscript $j = 1$ has been dropped for simplicity. Different approaches have been used to tackle the existence of a cross-term between the molecular reorientation and ODF [94–96]. In particular, they produce different cross-terms with opposite signs. The small cross-term of Freed is negative.

Another rotational model known as the anisotropic viscosity model [99,100] is very similar to the above model, but its main feature is in diagonalizing the rotational diffusion tensor in the laboratory frame defined by the director. The spectral densities are still given by Eq. (43), but the correlation times are now given by

$$\left[\tau_{mn}^{(j)}\right]^{-1} = \frac{6D_\beta}{b_{mn}^{(j)}} + m^2(D_\alpha - D_\beta) \tag{45}$$

where the rotational diffusion constants D_α, D_β denote, respectively, the precessional and tumbling motions of the long molecular axis with respective to the director. An extension to the anisotropic viscosity model is given by Vold and Vold [56] in which the rotation of the molecule about its long axis is also taken into account and assumed to be independent of the α- and β-motions with a diffusional constant D_γ. This so called 'third rate' model uses correlation times in the form of

$$\left[\tau_{mn}^{(j)}\right]^{-1} = \frac{6D_\beta}{b_{mn}^{(j)}} + m^2(D_\alpha - D_\beta) + \zeta(n)D_\gamma \tag{46}$$

where the function $\zeta(n)$ is $(1 - \delta_n)$ or n^2 if the γ-motion is described by the strong collision [97,98] or small step diffusion limit [70], respectively.

A simple composite model of slow motions and reorientations is the so called 'slowly relaxing local structure model' by Freed [99,100]. This model is good for nearly isotropic solutions that show locally ordered clusters, and the spectral densities are written in terms of three Lorentzians to account for the reorientation with a correlation time $\tau_0^{-1} = 6D(D_\perp = D_\parallel = D)$ and the slowly fluctuating component of the mean potential with a correlation time τ_x :

$$J_m(\omega) = \left[d_{00}^2(\beta_{\mathrm{M,Q}})\right]^2 \left\{c_{m0}\left[1 - \frac{a_{m0}b_{m0}\tau_0}{1 + \omega^2(b_{m0}\tau_0)^2}\right] + \tfrac{1}{5}(a_{m0})^2(b_{m0})^2 S_l^2 \times \left[\frac{\tau_x}{1 + \omega^2\tau_x^2} - \frac{\tau_0'}{1 + (\omega\tau_0')^2}\right]\right\}. \tag{47}$$

Here $S_l = \langle D_{00}^2 \rangle$ is the order parameter of the local structure and $(\tau_0')^{-1} = (\tau_x)^{-1} + (\tau_0)^{-1}$. Now $\tau_0' \simeq \tau_0$ as the correlation time τ_x for slowly fluctuating mean potential is much longer than τ_0. In the limit the spectral densities are independent of the projection index m (i.e. nearly 'isotropic' fluid), $a_{m0} = b_{m0} = 1$ and $c_{m0} = 1/5$, the above equation reduces to sum of two Lorentzians:

$$J(\omega) = \frac{1}{5}\left[d_{00}^2(\beta_{\mathrm{M,Q}})\right]^2 \times \left[\left(1 - S_l^2\right)\frac{\tau_0}{1 + \omega^2\tau_0^2} + S_l^2\frac{\tau_x}{1 + \omega^2\tau_x^2}\right]. \tag{48}$$

The same result has been obtained by Lipari and Szabo's 'model-free' approach [101]. This model-free approach has become popular among workers in the area of lyotropics and biomembranes.

3.3. Anisotropic translational diffusions

For spin-1/2 nuclei, dipolar interactions may be modulated by intramolecular (ODF, reorientation etc.) and/or intermolecular (SD) processes. In general, the intra- and inter-molecular processes can produce quite different T_1 frequency dispersion curves. In practice, NMR field cycling experiments are often needed to extend the frequency domain from those obtained in the MHz region using conventional spectrometers to the kHz regime for unambiguous separation (and identification) of different relaxation mechanisms. The Zeeman spin relaxation by anisotropic translational diffusions in various mesophases

has been considered by Žumer and Vilfan [65–67,102]. For the nematic phase, Žumer and Vilfan found the following expression for T_1

$$T_1^{-1}(\omega) = \frac{9}{8}\left(\frac{\mu_0\gamma^2\hbar}{4\pi}\right)^2 \frac{n\tau_\perp}{d^3} Q\left(\omega\tau_\perp, \frac{\langle r_\perp^2\rangle}{d^2}, \frac{D_\parallel^0}{D_\perp^0}\right) \tag{49}$$

where n is the number of spins per unit volume, $\langle r_\perp^2\rangle$ is the mean square jump length in the direction perpendicular to the long molecule axis, d is the distance of closest approach of two proton spins on neighboring molecules, $\tau_\perp$ is the correlation time for two successive jumps in the direction along $r_\perp$, Q is a dimensionless function which depends on the details of the diffusion process and on the spatial arrangement of molecules and $D_\parallel^0/D_\perp^0$, representing the SD anisotropy for a system with perfect order (i.e. $\langle P_2\rangle = 1$), is given in terms of the principal components of translational diffusion tensor $D_\parallel^t$ and $D_\perp^t$ [103]

$$\frac{D_\parallel^0}{D_\perp^0} = \frac{D_\parallel^t - \overline{D^0}(1-\langle P_2\rangle)}{D_\perp^t - \overline{D^0}(1-\langle P_2\rangle)} \tag{50}$$

with $\overline{D^0} = (D_\parallel^0 + 2D_\perp^0)/3$. In the limit $\omega\tau_\perp \ll 1$, Eq. (49) reduces to

$$T_1^{-1}(\omega) \propto C - (\omega\tau_\perp)^{1/2} \tag{51}$$

where C is a constant, in accordance with the Torrey's theory for translational SD in isotropic liquids [61,62,104]. Indeed Torrey's isotropic approximation has been used in the past to account for spin relaxation due to the translational diffusion in nematics [105]. Eq. (49) and its equivalent for smectic phases have recently been used to account for proton spin relaxation in LCs [106]. Although the T_1 relaxation by translationally diffusing molecules in N and SmA phases are quite similar [65,66], the particular structure of the twist grain boundary smectic A (TGB_A) presents a unique situation for molecules exhibiting translational SD [107]. TGB_A is a kind of frustrated SmA phase. Molecules crossing the grain boundary region from one smectic block to an adjacent one along the helical axis need to rotate by an angle $\Delta\alpha$ (the angle between adjacent blocks). This kind of roto-translation relaxation of spin-1/2 nuclei on neighboring molecules has been detected by a proton T_1 dispersion study in the compound $18FBTCO_1M_7$ [108].

3.4. Correlated internal bond rotations

Deuterium (^2H) NMR is particularly useful for studying conformational changes in flexible mesogens owing to its unique property of site specificity. One possible drawback is the necessity to selectively deuteriate LC molecules, which can be time-consuming and costly in terms of chemical syntheses. It is well known that deuterium NMR spectra in mesophases of aligned LCs show well-resolved quadrupolar doublets for different labeled sites. It is also clear that the orientational order and quadrupolar splittings for a molecule exhibiting many conformational states cannot be described by one single order matrix as in a rigid molecule. Thus, all possible conformations must first be generated using the rotational isomeric state (RIS) model of Flory [80]. Each conformer, due to its own shape anisotropy, has its own order matrix describing its orientational tendency in the nematic mean field. The problem becomes rather complex owing to the need to use a large number of order matrices to evaluate the splittings for all conformers, and then properly averaging these to give the observed quadrupolar splitting. To proceed, the orienting potential of a molecule due to its neighbors must be specified for each conformer. To avoid the problem of introducing too many adjustable parameters, the additive potential (AP) method, pioneered by Marcelja [109] and later refined by Emsley et al. [110], can be used to construct the potential of mean torque $U_{ext}(n,\Omega)$ for the nth conformer with orientation Ω with respect to the director. Here it is assumed that the molecule can be divided into a small number of rigid segments. Each segment is associated with an interaction tensor that is independent of the conformation. The interaction tensor $U_{ext}(n,\Omega)$ for the molecule in conformation n is calculated by transforming the segmental interaction tensors from their local frames into a common molecular frame and then adding them together. The total, anisotropic potential energy $U(n,\Omega)$ for the molecule in conformation n is given by

$$U(n,\Omega) = U_{int}(n) + U_{ext}(n,\Omega) \tag{52}$$

where $U_{int}(n)$, the internal energy, can usually be

approximated by $U_{\rm int}(n) = N_g E_{tg}$ with N_g being the number of *gauche* linkages in the chain and E_{tg} the energy difference between the *gauche* linkage and the *trans*. The equilibrium probability for finding the molecule in the n conformer is given by the Boltzmann statistics

$$P_n = \frac{1}{Z}\exp\left[-\frac{U_{\rm int}(n)}{kT}\right]Q_n \tag{53}$$

where the conformation-orientational partition function Z is

$$Z = \sum_n \exp[-U_{\rm int}(n)/kT]Q_n$$

and the orientational partition function Q_n is

$$Q_n = \int \exp[-U_{\rm ext}(n,\Omega)/kT]\mathrm{d}\Omega.$$

Now P_n is known if the potential of mean torque $U_{\rm ext}(n,\Omega)$ can be extracted from fitting the calculated quadrupolar splittings to the observed ones at a particular temperature in the mesophase. Furthermore, the order matrix of an 'average' conformer of the molecule can also be calculated [27]. As seen below, $U_{\rm ext}(n,\Omega)$ is needed to describe both the internal dynamics and overall molecular reorientation. Here we will outline our decoupled model for describing correlated internal motions using the master rate equation method. In this model, the conformational changes in the chain are assumed to be much faster than the overall motion and therefore independent of the molecular orientation because of their different time scales.

In order to account for the internal motion and reorientation of the molecule, one needs to transform from the PAS to the L frame (via $\Omega_{\rm PL}$) through successive coordinates ($\Omega_{\rm PI}$, $\Omega_{\rm IM}$, $\Omega_{\rm ML}$): the intermediate (I) frame, chosen to describe various conformations in the chain, is fixed with respect to the M frame. The correlation functions in Eq. (12) for $m = 1, 2$ can be written as

$$G_m(t) = \sum_n \sum_k \sum_{k'} D^2_{nk}(\Omega_{\rm IM}) D^{2*}_{nk'}(\Omega_{\rm IM}) g^R_{mn}(t) \times \left\langle D^2_{k0}(\Omega_{\rm PI}(0) D^{2*}_{k'0}(\Omega_{\rm PI}(t)\right\rangle \tag{54}$$

where $\langle D^2_{k0}(\Omega_{\rm PI}(0) D^{2*}_{k'0}(\Omega_{\rm PI}(t)\rangle$ denote internal correlation functions that describe conformational transitions in the chain with respect to the I frame, and $\overline{D^2_{k0}} = 0$ has been assumed. In writing down Eq. (54), we use the fact that conformational changes in the chain(s) are not coupled to the overall motion of the molecule. Moreover, in writing down $g^{\rm R}_{mn}(t)$ the rotational diffusion tensor was assumed to be the one for an average conformer. In other words, the diffusion tensors for different conformers do not deviate substantially from each other. For $m = 0$, there is an additional term in Eq. (54) which involves the internal correlation functions weighed by $\langle P_2\rangle^2 \delta_{n0}$ [71,72]. The internal correlation functions are given by

$$\left\langle D^2_{k0}(\Omega_{\rm PI}(0)) D^{2*}_{k'0}(\Omega_{\rm PI}(t))\right\rangle = \sum_{l,n} \exp\left[-\mathrm{i}k\alpha^l_{\rm PI}\right] d^2_{k0}\left(\beta^l_{\rm PI}\right) P_n \exp\left[-\mathrm{i}k'\alpha^n_{\rm PI}\right] \times d^2_{k'0}(\beta^n_{\rm PI}) p(l,t|n,0) \tag{55}$$

where $p(l,t|n,0)$ is a conditional probability for finding conformation l at time t given that at $t = 0$, the molecule has conformation n with equilibrium probability of occurrence p_n, $\beta^l_{\rm PI}$ and $\alpha^l_{\rm PI}$ are the polar angles of the principal axis of PAS (e.g. C–D bond) for the conformer l in the I frame. The conditional probability can be found by solving a master rate equation, which involves a transition rate matrix $\bar{\bar{R}}$. The original decoupled model [71,72] uses three phenomenological jump constants k_1, k_2 and k_3 to describe transitions among different conformations. Specifically, k_1, k_2 and k_3 are for the so-called one-bond, two-bond and three-bond motions. In general, there can be several jump constants for each type of bond motion [71,72]. For simplicity, we adopt only one jump constant for each type of bond rotation. Suppose the carbon–carbon backbone of a pentyl chain is in a configuration characterized by $\{ijklm\}$. The one-bond (k_1) motion is given by $\{ijklm\} \rightarrow \{ijklm'\}$, and the two-bond ($k_2$) motion is for $\{ijklm\} \rightarrow \{ijkl'm\}$ and $\{ijkl'm'\}$, i.e. one-bond and two-bond motions occur at the end of the chain. The three-bond (k_3) motion involves the interchanging two alternate (next-nearest-neighbor) bonds, viz. $\{ijklm\} \rightarrow \{ilkjm\}$. The latter motion produces no net translation of the attached chain, and has been thought to be a favorable process in ordered phases.

Table 1
Jump constants and rotational diffusion constants for liquid crystals based on the decoupled model at a particular temperature

Molecule	k_1 (s^{-1})	k_2 (s^{-1})	k_3(s^{-1})	$D_\perp$ (s^{-1})	$D_\parallel$ (s^{-1})
5CB (N)[a]	1.2×10^{11}	7×10^{14}	4×10^{12}	3.4×10^{7}	7.5×10^{8}
6OCB (N)[b]	4×10^{12}	2×10^{11}	4×10^{16}	3.4×10^{7}	2.8×10^{9}
8OCB (N)[c]	5.5×10^{12}	4.3×10^{12}	9.8×10^{16}	9.5×10^{7}	1.8×10^{10}
8OCB (SmA)[c]	1×10^{13}	3.5×10^{12}	9.8×10^{16}	6×10^{7}	6.5×10^{9}
8OCB/6OCB (SmA)[d]	1.5×10^{13}	2.8×10^{12}	4×10^{16}	3×10^{7}	2×10^{9}
8OBCB (RN)[e]	2×10^{15}	1.1×10^{12}	5×10^{17}	1.1×10^{8}	9×10^{9}
Azpac (N)[f]	2.5×10^{12}	1.1×10^{12}	6×10^{16}	2×10^{6}	2×10^{7}
HAT6 (D_{ho})[g]	5×10^{17}	4×10^{12}	9×10^{12}	3.8×10^{7}	1.1×10^{8}

[a] Pentylcyanobiphenyl, 291 K [122].
[b] Hexyloxycyanobiphenyl, 328 K [116].
[c] Octyloxycyanobiphenyl, 345 K (N), 333 K (SmA) [118].
[d] 72/28 wt% of 8OCB/6OCB, 312 K [120].
[e] Octyloxybenzoyloxy cyanobiphenyl, 377 K [119].
[f] Acetylacetonate derivative of cyclopalladated bis(hexyloxy)azoxybenzene, 362 K [121].
[g] Hexakis(*n*-hexyloxy) triphenylene, 351 K, $D_\perp \equiv D_\beta$ and $D_\parallel = D_\alpha$ (see text) [117].

The spectral densities for the C_i deuterons on the chain of an asymmetric top molecule can be obtained from Eq. (54) for $m > 0$ and for the case of the I frame being coincident with the M frame

$$J_m^{(i)}(m\omega) = \sum_n \sum_{n'} \sum_{j=1}^{N} \times \left(\sum_{l=1}^{N} d_{n0}^2\left(\beta_{\mathrm{PM}}^{(i)l}\right) \exp\left[-\mathrm{i}n\alpha_{\mathrm{PM}}^{(i)l} \right] x_l^{(1)} x_l^{(j)} \right) \times \left(\sum_{l'=1}^{N} d_{n0}^2\left(\beta_{\mathrm{PM}}^{(i)l'}\right) \exp\left[-\mathrm{i}n'\alpha_{\mathrm{PM}}^{(i)l'} \right] x_{l'}^{(1)} x_{l'}^{(j)} \right) \times \sum_k \frac{\left(A_{mnn'}^2\right)_k \left[\left(B_{mnn'}^2\right)_k + |\lambda_j| \right]}{m^2\omega^2 + \left[\left(B_{mnn'}^2\right)_k + |\lambda_j| \right]^2} \tag{56}$$

where $\beta_{\mathrm{PM}}^{(i)l}$ and $\alpha_{\mathrm{PM}}^{(i)l}$ are the polar angles for the C_i–D bond of the conformer l in the M frame fixed on the molecular core, $|\lambda_j|$ and $\vec{x}^{(j)}$ are the eigenvalues and eigenvectors from diagonalizing $N \times N$ $\bar{\bar{R}}$ (N is the number of possible conformations in the chain). The A and B coefficients are those shown in Eq. (38) except they are now generalized to an asymmetric top [57] in describing the molecular reorientation. Eq. (56) takes an additional term when $m = 0$ and for a symmetric top molecule, it is given by

$$J_m^{(i)}(m\omega) = \sum_n \sum_{j=1}^{N} \left| \sum_{l=1}^{N} d_{n0}^2\left(\beta_{\mathrm{PM}}^{(i)l}\right) \times \exp\left[-\mathrm{i}n\alpha_{\mathrm{PM}}^{(i)l} \right] x_l^{(1)} x_l^{(j)} \right|^2 \times \sum_k \frac{\left(A_{mn}^2\right)_k \left[\left(B_{mn}^2\right)_k + |\lambda_j| \right]}{m^2\omega^2 + \left[\left(B_{mn}^2\right)_k + |\lambda_j| \right]^2} + \delta_{m0}\langle P_2\rangle^2 \sum_{j=1}^{N} \left| \sum_{l=1}^{N} d_{00}^2\left(\beta_{\mathrm{PM}}^{(i)l}\right) x_l^{(1)} x_l^{(j)} \right|^2 / |\lambda_j|. \tag{57}$$

The decoupled model has successfully been used to understand the internal dynamics of flexible chain(s) in many different LCs studied by the proton [111] and deuteron [112–123] spin relaxation. Table 1 summarizes representative internal jump constants and rotational diffusion constants for LCs with different chain lengths including calamitics, discotics and metallomesogens. These studies have derived rather high values of k_3 (about 10^{17}–10^{18} s^{-1}), for the three-bond motion in some of the studied materials. In addition, one or more jump constants do not seem to show thermally activated behaviors in some LCs. In fact, the k_3 (or type I motion of Helfand [124]) motion should call for a high activation energy [125,126]

because several bonds must be activated almost simultaneously and hence a low value of k_3. Helfand has classified conformational transitions in the chain into three types: besides the type I motion, type III motion consists of one- and two-bond motions described above and type II motion also consists of two kinds, viz. $ttt \rightarrow g^{\pm}tg^{\mp}$ is a *gauche* pair production or a kink formation, and $ttg \rightarrow gtt$ is *gauche* migration [124]. The type II motion does not swing the chain but the chain does translate. Given that Helfand has discarded the type I motion [125,126] and in view of the high observed k_3 rates, the original decoupled model has recently been modified [127,128] by replacing the k_3 motions by the type II motion of Helfand. The jump rates k_g and $k_{g'}$ are for a *gauche* migration and *gauche* pair formation, respectively. The new decoupled model inevitably introduces an additional jump constant in describing internal chain dynamics. The transition rate matrix $\bar{\bar{R}}$ is now different, but the expression for spectral densities remains given by Eq. (56).

To describe quadrupolar splittings and internal dynamics, the following geometry has been adopted for an alkyloxy chain: the O–C_α bond is taken to be fixed on the phenyl ring plane with $\angle C_{ar}OC_\alpha = 126.4°$; ∠CCC, ∠CCH and ∠HCH are assumed to be 113.5, 107.5 and 113.6°, respectively. In constructing $U_{ext}(n, \Omega)$, the O–C bond is treated same as a C–C bond, and $\angle OCC = \angle CCC$ is assumed. The dihedral angles $\phi = 0, \pm 112°$ are for rotation about each C–C bond or the O–C bond to generate the three RIS. In anticipation of using the new decoupled model to longer chain molecules, we limit the number of conformations to those with relatively high probabilities. For instance, a hexyloxy chain which contains four or more *gauche* C–C bonds can be safely ignored, because they are energetically unfavorable. Even the conformations with two consecutive *gauche* C–C bonds (i.e. $g^{\pm}g^{\pm}$ and $g^{\pm}g^{\mp}$) can be ignored. Going to an octyloxy chain, conformations with four *gauche* C–C bonds are allowed, while for a decyloxy chain conformations with up to five *gauche* C–C bonds are now allowed. With these assumptions, $N =$ 43, 171 and 683 for molecules containing a hexyloxy, octyloxy and decyloxy chain, respectively.

In setting up the $\bar{\bar{R}}$ matrix among the N conformations, the following conditions are imposed [127]: (i) no direct transition between a g^+ and g^- states is allowed as this costs too much energy, (ii) transitions between *gtgtt* and *tgtgt* cannot proceed directly as these also cost too much energy (however, $gtgtt \rightleftharpoons ttttt \rightleftharpoons tgtgt$ are possible), and (iii) no three-bond (k_3) motion is allowed. For example, there is a total of 584 transitions for $\bar{\bar{R}}$ in the case of 8OCB. Among the 292 forward transitions, there are 86 type III motions about the C_6–C_7 bond (k_1 motion), 42 type III motions about the C_5–C_6 bond (k_2 motion), and 164 type II motions. For the latter type, 82 transitions are for the *gauche* migration and 82 transitions are for the kink formation.

If the local interaction tensors for the aromatic core and the C–C segment are assumed to be cylindrically symmetric, their unique components X_a and X_c will form the model parameters in the AP method for fitting the observed quadrupolar splittings. Specifically, the quadrupolar splitting $\Delta\nu_i$ for the C_i deuterons is calculated from

$$\Delta\nu_i = \frac{3}{2}\left(\frac{e^2qQ}{h}\right)\sum_{n=1}^{N} p_n S_{bb}^{n,i} \tag{58}$$

where $S_{bb}^{n,i}$, the segmental order parameter for the C_i–D bond (along the b axis) of the molecule in the conformation n, is given by

$$S_{bb}^{n,i} = \sum_{\alpha}^{x,y,z} S_{\alpha\alpha}^{n} \cos^2 \theta_{\alpha b}^{n,i} \tag{59}$$

with $S_{\alpha\alpha}^{n}$ denote the principal components of the order matrix for the n conformer, and $\theta_{\alpha b}^{n,i}$ denotes the angle between the C_i–D bond of the n conformer and the α axis of the principal axes of $U_{ext}(n, \Omega)$. In the PAS, $S_{\alpha\alpha}^{n}$ can be evaluated in a manner described for a rigid biaxial particle [129]. The potential of mean torque, parameterized by X_a and X_c, can therefore be mapped out at each temperature from fitting the quadrupolar splittings obtained in the mesophase of LCs.

3.5. Total relaxation rates

Since different molecular processes may simultaneously contribute to spin relaxation in LCs, the relaxation rates due to various relaxation mechanisms are additive if the motions can be uncoupled on the basis of sufficiently different correlation

Table 2
Jump constants and rotational diffusion constants for liquid crystals based on the Helfand types II and III motions in the decoupled model

Molecule	k_1 (s^{-1})	k_2 (s^{-1})	k_g (s^{-1})	k'_g (s^{-1})	$D_\perp$ (s^{-1})	$D_\parallel$ (s^{-1})
6OCB (N)[a]	5×10^{12}	2×10^{11}	2×10^{12}	9.5×10^{13}	4×10^{7}	2×10^{9}
8OCB (N)[b]	1.2×10^{12}	7×10^{13}	2×10^{12}	2.8×10^{13}	1×10^{8}	1×10^{10}
8OCB (SmA)[b]	1.2×10^{12}	1.8×10^{13}	1.9×10^{12}	1×10^{13}	7.5×10^{7}	6×10^{9}
8OCB/6OCB (SmA)[c]	1.4×10^{12}	1×10^{12}	3×10^{12}	4×10^{11}	3.6×10^{7}	1.9×10^{9}
8OBCB (RN)[d]	4.8×10^{12}	1.1×10^{13}	7.4×10^{12}	1.7×10^{13}	1.4×10^{8}	7.4×10^{9}
10B1M7 (SmA)[e]	1.2×10^{13}	2.8×10^{14}	2.85×10^{13}	2.9×10^{12}	3.4×10^{7}	7.6×10^{9}

[a] 328 K [128].
[b] 345, 333 K (SmA) [131].
[c] 312 K [131].
[d] 377 K [131].
[e] 1-Methylheptyl 4′-(4-*n*-decyloxybenzoyloxy)biphenyl-4-carboxylate, 381 K [132].

times [18]

$$T_1^{-1} = T_{1SD}^{-1} + T_{1ODF}^{-1} + T_{1R}^{-1} + T_{1X}^{-1} \tag{60}$$

where T_{1SD}^{-1} denotes the relaxation rate due to translational SD, T_{1R}^{-1}, the relaxation rate due to MR and/or internal motions, and T_{1X}^{-1}, the cross-term contribution between the MR and ODF. For deuterons, T_{1SD}^{-1} is zero because of the intramolecular nature of quadrupolar interaction. When the time scale argument for superimposing different relaxation mechanisms becomes untenable, the treatment of spin relaxation becomes more complex. There is one model [130] which does not use the time scale separation when the molecular reorientation has slowed down to be comparable to the distribution of correlation times of ODF.

4. Relaxation in thermotropics

In this section, we survey some recent relaxation studies of thermotropic LCs, among which are deuterium NMR studies carried out in our laboratory. Relaxation studies by means of other nuclei such as proton and ^{13}C will be briefly described to reflect current interests in these materials. In fact, ^{13}C spin relaxation studies of LCs have been neglected in comparison with ^{2}H and ^{1}H relaxation studies.

4.1. Deuteron studies

We begin by making some general remarks regarding the new decoupled model for LCs [127,128,131]. In anticipating its usage to a longer-chain chiral molecule, 1-methylheptyl 4′-(4-*n*-decyloxy-benzoyloxy) biphenyl-4-carboxyate (10B1M7) [132], the number of conformations has been significantly reduced using the assumptions given above. In spite of this limitation, the quadrupolar splittings and relaxation data of several LCs can be satisfactorily interpreted, resulting in reasonable order parameters, rotational diffusion and internal jump constants. Table 2 summarizes typical values at a particular temperature in several studied LCs. It is clear that all internal jump rates k_1, k_2, k_g and k'_g are smaller than $1 \times 10^{14}\ s^{-1}$. The rotational diffusion constants for the same LC obtained from the original and modified decoupled models are very similar (see Tables 1 and 2), i.e. regardless of whether k_3 or type II motions were used. In other words, the overall motion is relatively well defined. It is interesting to note that the tumbling diffusion constant $D_\perp$ is inversely related to the rotational viscosity coefficients based on statistical mechanical approaches (SMA) [133]. The temperature dependencies of the rotational viscosity coefficients for 8OCB have recently been studied based on the SMA in combination with the NMR data of this compound [134], and found to agree with the experimentally measured values. Such a study has lent support to the applicability of the decoupled model in interpreting relaxation data due to the overall and internal dynamics in LCs. For discotic mesogens like HAT6 (see Table 1), the tumbling motion away and towards the director ($D_\beta \equiv D_\perp$) is

Table 3
Activation energy (in kJ/mol) for jump constants and rotational diffusion constants for liquid crystals based on the new decoupled model

Molecule	$E_a^{k_1}$	$E_a^{k_1}$	$E_a^{k_g}$	$E_a^{k'_g}$	$E_a^{D_\perp}$	$E_a^{D_\parallel}$
6OCB	[a]	49.7	62.1	[b]	35.6	36.6
8OCB	[b]	130.7	3.9	89.4	30.4	60.9
8OCB/6OCB	[b]	62.5	3.2	89	40.8	40.7
8OBCB	28.7	18.5	16.7	149.3	17.7	51.4
10B1M7	31.1	35.9	44.6	59.1	9.5	49.6

[a] k_1 is modeled by a simple power series in temperature.
[b] Jump rate is independent of temperature.

Table 4
The prefactor A and high frequency cutoff derived from deuterium NMR relaxation studies

Molecule	A ($s^{1/2}$)	$\omega_c/2\pi$ (MHz)
6OCB (N)[a]	9.9×10^{-6}	30 (at 340 K)
8OCB (N)[a]	9.9×10^{-6}	30 (at 350 K)
8OCB/6OCB (N)[b]	6.7×10^{-6}	90 (at 350 K)
8OBCB (RN)[c]	4.7×10^{-6}	35 (at 363 K)
1O.4 (N)[d]	1.8×10^{-5} (at 306 K)	10
5O.7 (SmA)[d]	1.8×10^{-6} (at 333 K)	145 (at 348 K)
4O.8 (N)[d]	3.9×10^{-6} (at 340 K)	300 (at 350 K)
5CB (N)[e]	2.4×10^{-5} (at 299 K)	1

[a] Ref. [128].
[b] Ref. [120].
[c] Ref. [119].
[d] *p*-Alkyloxybenzylidene-*p*-*n*-butylaniline (nO.m) [77].
[e] Ref. [110].

disruptive to the columnar structure and has smaller rates in comparison to D_α ($\equiv D_\parallel$), the spinning motion of the molecule about the director, in the 'anisotropic viscosity' model [99,100]. Deuterium NMR investigations of the core dynamics of 1-fluoro-2,3,7,10,11-hexahexyloxytriphenylene (F-HAT6) [135] and rufigallol [136] also reveal the same behavior. At 357 K, the rotational viscosity coefficients of HAT6 and F-HAT6 inferred from values of D_β are nearly identical, while those of rufigallol are larger by a factor of two to three.

To achieve sensible model parameters of the decoupled model, it is necessary to include spectral density parameters from different sites, at more than one Larmor frequency and as a function of temperature. Indeed, a global target analysis [114] has been shown to achieve this goal. In this approach, the spectral densities at different Larmor frequencies and many different temperatures are fitted simultaneously by minimizing the sum squared percentage error F

$$F = \sum_k \sum_\omega \sum_i \sum_m \left[\frac{J_m^{(i)}(m\omega)_{\exp\, t} - J_m^{(i)}(m\omega)_{\mathrm{calc}}}{J_m^{(i)}(m\omega)_{\exp\, t}} \times 100 \right]^2 \tag{61}$$

where $J_m^{(i)}(m\omega)_{\mathrm{calc}}$ are given by Eq. (56) and the sum over i covers all the measured deuteron sites, the sum over ω is for two Larmor frequencies (in our case), the sum over k is to cover all the selected temperatures, and $m = 1$ and 2. To get some idea on the temperature behaviors of target model parameters, individual target analyses (i.e. analyze spectral densities at each temperature) must first be carried out. The rotational diffusion and jump constants can often be approximated by simple Arrhenius relations

$$D_j = D_j^0 \exp\left[-E_a^{D_j}/RT\right] \tag{62}$$

$$k_i = k_i^0 \exp\left[-E_a^{k_i}/RT\right] \tag{63}$$

$$k_g = k_g^0 \exp\left[-E_a^{k_g}/RT\right] \tag{64}$$

$$k'_g = k_g^{'0} \exp\left[-E_a^{k'_g}/RT\right] \tag{65}$$

where $j = \perp$ or $\parallel$, $i = 1$ or 2, D_j^0, k_i^0, k_g^0 and $k_g^{'0}$ are the pre-exponential constants and E_a with an appropriate superscript is the corresponding activation energy. It is well known that the pre-exponential constant and its corresponding activation energy are highly correlated with a correlation coefficient near one [115]. Thus, Eqs. (61)–(64) are rewritten to remove the pre-exponentials by using the target parameters at a particular chosen temperature. Table 3 summarizes the activation energies for the LCs listed in Table 2. As seen in this table, the activation energy for tumbling motion $D_\perp$ is often found to be smaller than that for the spinning motion ($D_\parallel$). Although this is an unphysical result for rod-like mesogens, it is a well known difficulty [112,137,138] of NMR relaxation studies in pinning down the motion of the long molecular axis about a short axis of the molecule. Another observation is that the jump constants tend to follow thermally activated behavior or show weak (no) temperature dependences. Thus, it is tempting to

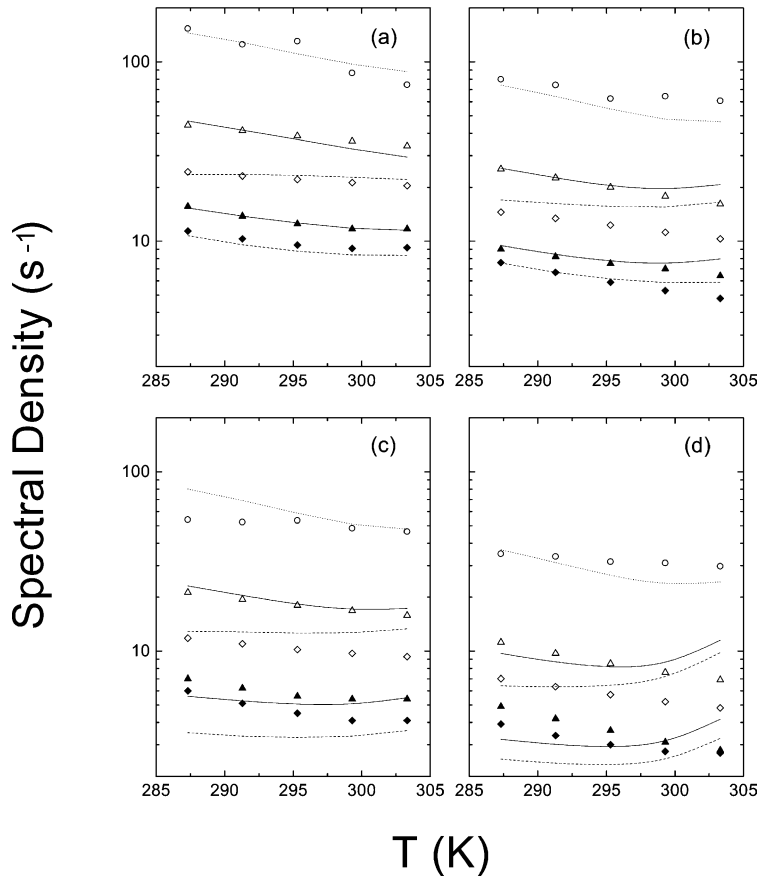

Fig. 1. Experimental (smoothed data) and calculated (lines) spectral densities of 5CB-d_{15}. The open circles denote $J_0(0)$, the open triangles and diamonds denote $J_1(\omega)$, while the closed triangles and diamonds denote $J_2(2\omega)$. The triangles and diamonds represent data at 15.3 and 46 MHz, respectively. (a) and (b) are for C_1 and C_2, while (c) and (d) for C_3 and C_4, respectively. Solid and dashed lines are for 15.3 and 46 MHz, while dotted lines are for $J_0(0)$.

conclude that the new decoupled model is more preferred in describing the conformational change within flexible chain(s) of LCs.

Although ODF is known to contribute more effectively in the kHz regime, it is found that in certain nematic phases ODF can contribute up to 30% of the total relaxation rate even at 15 MHz [88,116,139,140]. At this frequency, the ODF contribution in smectic phases is, however, non-existent [139,140]. Using the new decoupled model (Table 2), director fluctuation was found necessary to fit the T_1 data in the nematic phase of 6OCB, 8OCB and a mixture of 72/28 wt% 8OCB/6OCB. For this contribution, an additional adjustable parameter is A, the prefactor given in Eq. (35). The high frequency cutoff $\omega_c/2\pi$ is set at a certain value and is assumed to depend linearly on temperature such that $\omega_c/2\pi$ in the SmA phase (if it exists in the phase sequence) is small enough to make the cutoff function $U(x)$ in Eq. (34) equal to zero. In this manner, the temperature dependence of ODF comes solely from ω_c. Since A and ω_c are highly correlated, a different initial ω_c is always possible with of course a different A value. Table 4 summarizes some A values, which are not intended for direct comparison among different LCs. Indeed, in earlier studies of 1O.4, 5O.7 and 4O.8 both A and/or ω_c are assumed to be temperature-dependent.

The T_{1Z} and T_{1Q} data in the nematic phase of 1O.4 and 5CB can be interpreted without ODF. To shed light on the ODF in these materials, T_2 given in Eq.

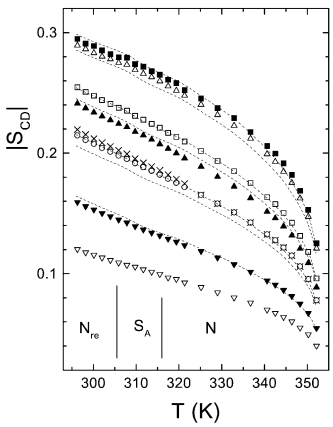

Fig. 2. Plot of quadrupolar splittings of 8OCB in a 8OCB/6OCB mixture versus the temperature. Solid squares, uptriangles, × and downtriangles denote C_1, C_3, C_5, and C_7 sites, respectively. Open uptriangles, squares, circles and downtriangles denote C_2, C_4, C_6, and C_8 sites, respectively. The solid curves are the theoretical calculations for C_1 to C_7 starting from the top. Note that the experimental splittings of C_3 and C_4 are reversed from those predicted by the AP method.

(20) can be measured using a quadrupolar echo pulse train at 46 MHz [141] to give additional spectral densities $J_0^{(i)}(0)$ for the methylene deuterons in the chain. By including the second-order contribution of ODF in $J_0^{(i)}(0)$, both T_1 and T_2 relaxation data can be satisfactorily interpreted in 1O.4 [88,141] and 5CB [122] using the original decoupled model. Fig. 1 reproduces the spectral densities $J_0^{(i)}(0)$, $J_1^{(i)}(\omega)$ and $J_2^{(i)}(2\omega)$ for the methylene deuterons in the nematic phase of 5CB. The number of conformations used for the pentyl chain was $N = 81$. The potential of mean torque (X_a and X_c) and the order parameters of the average conformer were obtained from the analysis of quadrupolar splittings [123] using the AP method. A global target analysis [122] of these data together with the $J_1^{(R)}(\omega)$ and $J_2^{(R)}(2\omega)$ of the ring was carried out. The $J_0(0)$ due to ODF given in Eq. (31) had to be modified by introducing a low cutoff frequency (ω_1) in order to remove the divergence as $\omega \rightarrow 0$ [84]. The high and low frequency cutoffs in this study were taken as 1 MHz and 98 Hz, respectively. The low frequency cutoff was estimated from the magnetic coherence length ξ and viscoelastic constants K and η. While the two-bond (k_2) motion was found to be nearly constant, the three-bond (k_3) motion was determined to have an activation energy of 51.9 kJ/mol. The one-bond (k_1) motion was found to have increasing rates with decreasing temperature. The calculated spectral densities are shown as curves in

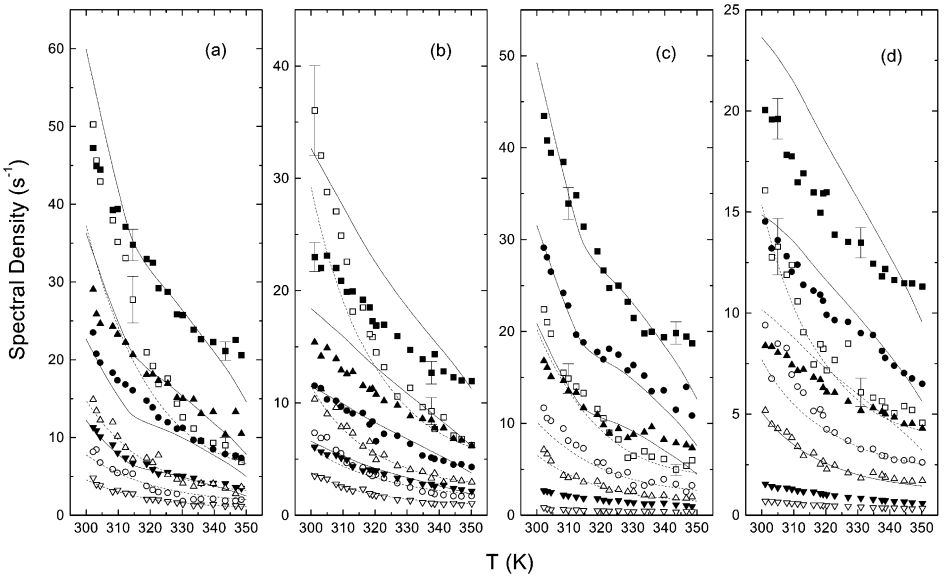

Fig. 3. Plots of spectral densities versus the temperature in a 8OCB/6OCB mixture at 15.1 MHz ((a) and (c)) and 46 MHz ((b) and (d)). Closed symbols denote $J_1^{(i)}(\omega)$ and open symbols denote their corresponding $J_2^{(i)}(2\omega)$. (a) Squares, uptriangles, circles and downtriangles denote data of C_1, C_3, C_5 and C_7, respectively; (b) same as (a); (c) squares, circles, uptriangles and downtriangles denote data of C_2, C_4, C_6 and C_8, respectively; (d) same as (c). Solid and dashed curves denote calculated spectral densities J_1 and J_2, respectively.

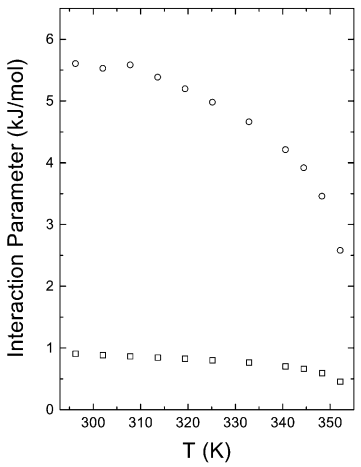

Fig. 4. Plots of interaction parameters X_a (circles) and X_c (squares) versus the temperature for 8OCB in a 8OCB/6OCB mixture.

Fig. 1. The activation energies for molecular reorientations are $E_a^{D_\perp} = 37.3\,\mathrm{kJ/mol}$ and $E_a^{D_\parallel} = 42.6\,\mathrm{kJ/mol}$. It was also clear that the molecular reorientation contributions to experimental $J_0^{(i)}(0)$ amount to between 21 and 30% for various methylene deuterons in 5CB at 295 K. Thus, with the additional contribution from the second-order ODF contribution $J_0^{(i)}(0)$ appeared to be reasonably explained.

As an illustrative example of our new decoupled model, the analyses of deuterium quadrupolar splittings and T_1 data in the N, SmA and re-entrant

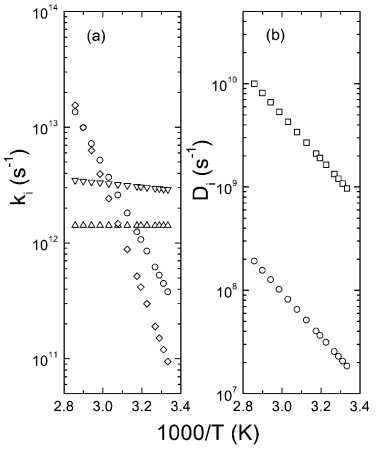

Fig. 5. Plots of (a) jump rate constants k_1 (uptriangles), k_2 (circles), k_g (downtriangles) and k_g' (diamonds), as well as (b) rotational diffusion constants $D_\parallel$ (circles) and $D_\perp$ (squares) as a function of the reciprocal temperature in a 8OCB/6OCB mixture.

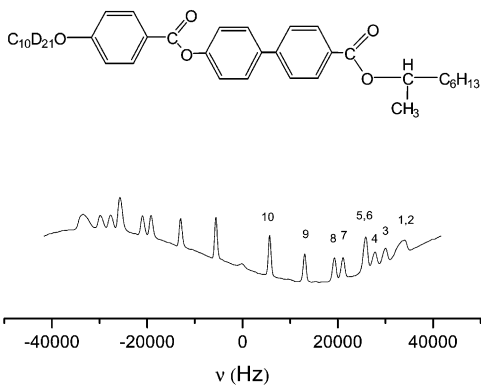

Fig. 6. Typical deuterium NMR spectrum in the SmA phase of 10B1M7-d_{21} and its molecular structure.

nematic (RN) phases of a chain-deuterated 8OCB-d_{17} in 28% by wt protonated 6OCB mixture are given. Figs. 2 and 3 reproduce the quadrupolar splittings and spectral densities data reported before [120], respectively. Using the AP method and Eq. (58), the calculated quadrupolar splittings are shown in Fig. 2 as solid curves. The AP method cannot reproduce the tentative assignment of $\Delta\nu_4 > \Delta\nu_3$ in 8OCB. However, the derived $U_{ext}(n, \Omega)$ in terms of X_a and X_c(see Fig. 4) and the order parameters of the average conformer are quite good for describing the internal and overall motions of 8OCB in this mixture. The $\langle P_2 \rangle$

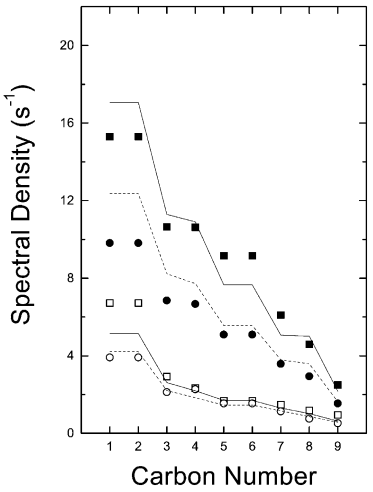

Fig. 7. Variation of the spectral densities $J_1(\omega)$ (solid symbols) and $J_2(2\omega)$ (open symbols) with the deuteron positions in the SmA phase of 10B1M7. Squares and circles denote data from 15.1 and 46 MHz, respectively. Solid and dashed lines are corresponding calculated spectral densities.

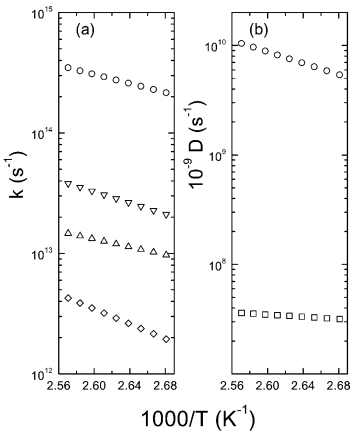

Fig. 8. Plots of (a) jump rate constants k_1 (uptriangles), k_2 (circles), k_g (downtriangles) and k'_g (diamonds), as well as (b) rotational diffusion constants $D_{\|}$ (circles) and $D_{\perp}$ (squares) as a function of the reciprocal temperature in 10B1M7.

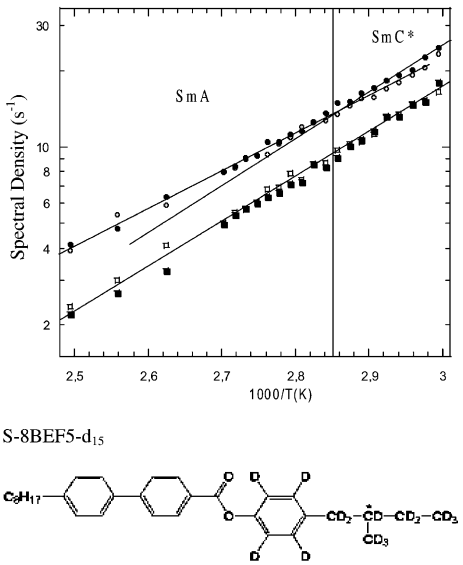

Fig. 9. Experimental spectral densities of the aromatic deuterons in the SmA and SmC* phases of 8BEF5. Circles and squares denote experimental $J_1(\omega)$ and $J_2(2\omega)$, respectively. Solid and open symbols refer to two distinct deuterons on the ring. Lines are drawn to highlight possible changes in the trend at the SmA–SmC* transition. The chemical structure of 8BEF5 is also given.

value ranges between 0.65 (295 K) and 0.3 (at clearing temperature T_C), while $\langle S_{xx} - S_{yy} \rangle$ is of the order 0.026 indicating the molecular biaxiality of the average conformer of 8OCB is indeed fairly small. As seen in Fig. 3, the values of $J_1^{(i)}(\omega)$ show substantial frequency dependencies at all carbon sites, while $J_2^{(i)}(2\omega)$ show small frequency dependencies. As in the pure 8OCB sample [128], the 'slow' molecular reorientation can account for the observed frequency dependences in $J_1^{(i)}(\omega)$ and $J_2^{(i)}(2\omega)$ in the SmA and RN phases. ODF is needed as an additional relaxation mechanism in the high temperature N phase. Using Eq. (56) for all the mesophases and Eqs. (32) and (33) in the N phase only, a global target analysis (using 14 different temperatures to cover all the phases) was carried out while noting that phase transitions did not seem to affect the validity of Eqs. (62)–(65). The calculated spectral densities for C_1 to C_7 are shown as curves in Fig. 3. Although systematic deviations between calculated and experimental spectral densities do exist, the overall fits are quite acceptable with a quality factor Q

$$Q = \frac{\sum_k \sum_\omega \sum_i \sum_m \left[J_m^{(i)}(m\omega)_{\text{calc}} - J_m^{(i)}(m\omega)_{\text{exp } t} \right]_k^2}{\sum_k \sum_\omega \sum_i \sum_m \left[J_m^{(i)}(m\omega)_{\text{exp } t} \right]^2}$$

of 1.8%. The ODF prefactor and $\omega_c/2\pi$ are given in Table 4. To achieve $U(x) = 0$, $\omega_c/2\pi$ was set at 3 MHz just below the N–SmA phase. In the present analysis, a total of 392 spectral densities was used to obtain eleven global target parameters (k_1 was kept independent of temperature). The derived jump and rotational diffusion constants are plotted as a function of the reciprocal temperature in Fig. 5.

To indicate the relative importance of ODF in the N phase of 8OCB/6OCB, we observe that at the high end of the N phase (350 K), the ODF contributions account for 30–35% of $J_1^{(i)}(\omega)$ at 15.1 MHz (about 14–16 at 46 MHz). At the N–SmA transition, the ODF contributions at 15.1 MHz amount to 1.5–2% of $J_1^{(i)}(\omega)$ because of the vanishing $U(x)$. As seen in Table 4, ODF in the RN phase of a high T_c (513 K) LC 8OBCB is non-zero, which is contrary to the finding in the RN phase of 8OCB/6OCB. We believe that the different ODF behaviors in the two RN phases of these materials simply reflect the differences in the viscoelastic coefficients due to their very different temperature ranges. Thus our studies seem to indicate that N and RN phases behave the same in terms of molecular dynamics. So far deuterium NMR studies have mainly focused on uniaxial phases, including the

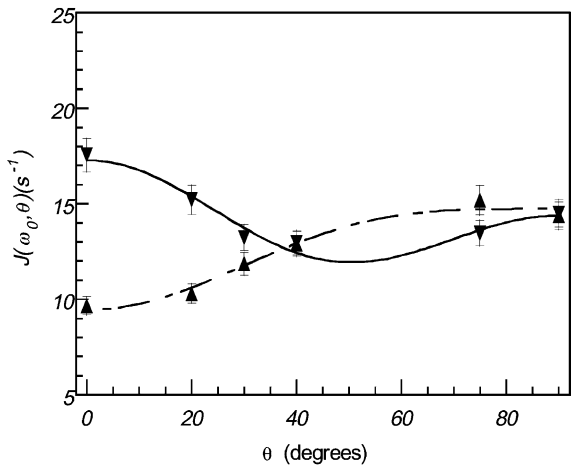

Fig. 10. Experimental $J_1(\omega,\theta)$ (downtriangles) and $J_2(2\omega,\theta)$ (uptriangles) at 15 MHz and 335 K as a function of θ, the angle between the director and the external magnetic field. Solid and dashed curves are the corresponding fitting curves (reproduced from Ref. [149] with the permission of the authors).

smectic B (SmB) phase of a smectogen [115]. The $D_\perp$ values in the SmB phase of *p*-hexyloxybenzylidene-*p'*-fluoroaniline are of the order 10^5 s^{-1}. Also there is a drastic change in the motional anisotropy ($D_\parallel/D_\perp$) at the SmA–SmB transition. This is not unreasonable as molecules are going from the 'liquid' layers in the SmA phase to a close hexagonal packing within the SmB layers.

The decoupled model has recently been applied to a longer chain chiral mesogen 10B1M7. Chiral mesogens like 10B1M7 are interesting as they often show ferroelectric (FLC) and antiferroelectric (AFLC) phases as well as extraordinary subphases [142,143]. The achiral chain of 10B1M7 is deuterated. Fig. 6 shows a typical deuterium NMR spectrum of 10B1M7-d_{21} and its molecular structure. The quadrupolar splittings were modeled by the AP method. The $\langle P_2\rangle$ of the average conformer ranges between 0.68 at T_c and 0.76 at 373 K. The achiral chain has been studied by deuterium spin relaxation in the SmA phase at 15.1 and 46 MHz. The chiral phases (SmC^*, SmC^*_{ferri}, SmC^*_{anti}) below the SmA phase were not studied because of excessive broadening of doublets for those deuterons near the beginning of the achiral chain. For 683 conformations in the achiral chain of 10B1M7, a total of 2776 transitional elements exists in the rate matrix $\bar{\bar{R}}$. Among the 1388 forward transitions, there are 342 type III motions about the C_8-C_9 bond (k_1 motions), 170 type III motions about the C_7-C_8 bond (k_2 motions), 438 transitions for the *gauche* migration and 438 transitions for the kink formation. The spectral density data [132] were successfully fitted to the calculated spectral densities with a Q value of 2.8%. Fig. 7 shows the site dependence of spectral densities at 381 K in the SmA phase of 10B1M7. The agreement between calculated and experimental spectral densities is relatively poor for C_1 and C_2, partly due to the overlap of their spectral lines (see spectrum) resulting in the inability to separately measure their individual spectral densities. The model parameters are summarized in Fig. 8 and their values at 381 K also appear are in Table 2. The activation energies $E_a^{D_\perp}$, $E_a^{D_\parallel}$, $E_a^{k_1}$, $E_a^{k_2}$, $E_a^{k_g}$, and $E_a^{k'_g}$ are 9.5, 49.6, 31.1, 35.9, 44.6 and 59.1 kJ/mol, respectively. It is interesting to compare both the jump constants and rotational diffusion coefficients for 10B1M7 with those of 8OCB in Fig. 5 even though these two compounds differ in their molecular structures and the lengths of studied side-chains. The diffusional anisotropy $D_\parallel/D_\perp$ seems to be larger for 10B1M7 than for 8OCB. This may simply reflect the larger size of the former molecule. When comparing the internal jump constants of these two mesogens, except k'_g the other three jump constants of 10B1M7 are about an order of magnitude larger than the corresponding values of 8OCB. The faster jump constants in 10B1M7 are likely due to its higher temperature range. No particular trend can be observed when comparing the activation energies for the individual jump processes of these two mesogens.

The increasing interest in understanding the structure and polar properties of chiral smectogens is reflected by recent relaxation studies using ^2H [142,144] and ^{13}C [145] probes. Veracini and coworkers have carried out deuterium relaxation studies in two members of a homologous series S-[4-(2-methylbutyl)phenyl]-4′-*n*-alkylbiphenyl carboxylate (nBEF5)]. The various relaxation times and corresponding spectral densities of 7BEF5 and 8BEF5 show no discontinuity in going from the non-tilted to the tilted smectic phase, indicating the reorientation processes in the MHz region show no drastic changes at the transition. Fig. 9 reproduces the experimental spectral densities of the aromatic deuterons of 8BEF5

in the SmA and SmC* phases [144]. As seen in this figure, the only change is a slight increase of the slope for $J_1(\omega)$ of the aromatic deuterons in going from the SmA to the SmC* phase. A quantitative analysis of the data from the aromatic and first methylene deuterons in the chiral chain was carried out in the SmA phase. However, the relaxation data in the SmC* phase still await a proper theoretical model for the chiral tilted phase before one can attempt to analyze them quantitatively. It is interesting to note that the internal rotations of the ring and the first methylene group in the chiral chain of 8BEF5 are found to be geared with the same activation energy and more or less the same diffusional rates [144]. Also these internal rotations about their respective axes can better be described by the small step diffusion model than the strong collision model.

It has been shown that when relaxation data at one frequency and/or of only a few deuterons are available, there is a high indeterminacy of $D_\perp$ [146]. Hence, the testing of motional models should be done with spectral densities measured at several Larmor frequencies. This, however, requires either field cycling experiments which are technically more demanding for deuterons, or conventional spectrometers at different magnetic fields, which may not be readily available. The problem may partly be overcome by exploiting the orientational dependencies of the spectral densities on the director with respect to the external magnetic field (see Eqs. (28)–(30). For example, $J_1(\omega, \Omega)$ contains three different crystal-frame spectral densities $J_0(\omega)$, $J_1(\omega)$ and $J_2(\omega)$ in uniaxial phases. By measuring $T_{1Z}(\Omega)$ and $T_{1Q}(\Omega)$ in the SmA phase of a ring deuterated 4-4′-di-*n*-octylazoxybenzene (OAB) [147,148] as a function of θ, Veracini and co-workers obtained spectral densities $J_1(\omega, \theta)$ and $J_2(2\omega, \theta)$ [149] which are reproduced in Fig. 10. To obtain the solid and dashed curves in this figure, six crystal-frame spectral densities ($J_m(\omega)$, $J_m(2\omega)$ where $m = 0, 1, 2$) must be calculated based on the reorientation motion ($D_\parallel$ and $D_\perp$) and internal ring rotation (D_R) about its para axis. Hence even at a single Larmor frequency, the data at six different orientations of the sample (Fig. 10) allow the separation of the six crystal-frame spectral densities. Three diffusion constants were determined [149] based on eight crystal-frame spectral densities (6 from 15 MHz and 2 from 46 MHz). $D_\parallel$ and D_R were found to be about $10^9\ s^{-1}$, three orders of magnitude higher than $D_\perp$, in the SmA phase of OAB. To date, there is no reported experimental study of biaxial spectral densities given in Eqs. (28)–(30). In principle, they can be determined by similar approaches in biaxial mesophases (e.g. SmC and SmG). Indeed, spin relaxation in smectic C phases has not been well-studied and often treated [150] by ignoring the 'small' phase biaxiality.

Interesting problems exist when considering spin relaxation of LCs confined in cylindrical cavities of Anopore membranes, in porous glasses and in embedded polymer network. Vilfan and co-workers have tackled this problem by carrying out deuteron T_1 and T_2 measurements [151,152]. Such measurements can provide information on the effect of spatial constraints on the molecular mobility and surface-induced order in certain enclosures. In these works, only the methylene protons at C_α of the cyanobiphenyl are replaced by deuterons for spectral simplicity, and the effect of LC–surface interactions is examined. For 5CB confined to porous glass of different pore sizes, there is no significant slowing-down of rotational or translational diffusion at the wall [152]. The finding is consistent with dielectric relaxation studies which show that $D_\perp$ remains unchanged in cylindrical channels of Anopore membranes having a diameter up to 0.2 μm with respect to the bulk sample [153].

There are several recent deuteron spin relaxation studies of liquid crystal polymers (LCP) [154,155]. Deuterated phenyl rings, located in the main chain of a main-chain/side-chain LCP and in the side chain of a LC copolymer, were employed to probe the phenyl ring dynamics. In the SmA phase of the main-chain/side-chain LCP, orientation dependencies of $J_0(0)$, $J_1(\omega)$ and $J_2(2\omega)$ were experimentally measured by means of T_1 and T_2 measurements. To reproduce the temperature and orientational dependencies of $J_m(m\omega)$, it was found that besides internal ring rotations and the overall rotational diffusion, an additional low amplitude torsional motion of the polymer about the main chain axis must be included. The internal ring rotation is treated as a diffusive process modulated by a twofold symmetric potential [154]. In the LC copolymer, both SmA and SmC* phases exist. At a magnetic field of 7 T, the mesogen

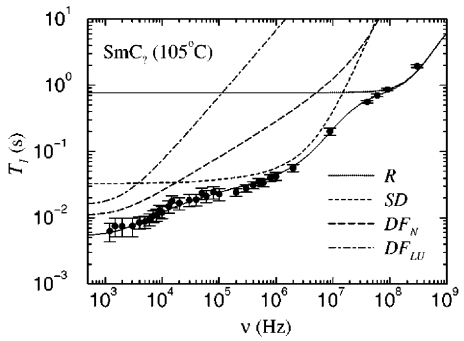

Fig. 11. Proton T_1 frequency dispersion in the SmC_2 phase of DB_8Cl. Various relaxation contributions are also given in the diagram (reproduced from Ref. [106] with the permission of the authors).

long axes are aligned along the magnetic field in the SmC* phase giving helix unwinding (i.e. a uSmC* phase) in this phase. By modeling $J_m(m\omega)$ as a function of temperature in both mesophases, it was found that the overall motion of the copolymer could be described by the anisotropic viscosity model [99], while the internal ring rotation is best described by small step rotation diffusion about the para axis. The ring diffusion constant has an Arrhenius temperature dependence, but with an activation energy distribution which is modeled by a Gaussian distribution. The study thus indicates a remarkable degree of dynamic heterogeneity in the copolymer. It should be noted that in this study the uSmC* phase has been treated by ignoring any phase biaxiality and its effect on the spin relaxation.

In summary, deuteron spin relaxation studies have been shown to be extremely useful for understanding collective and individual motions of thermotropic mesogens. At present, the relaxation problem involving internal bond rotations can only be tackled by means of deuterium NMR. In particular, the decoupled model appears to be well tested in flexible LCs, at least in uniaxial mesophases. Spin relaxation due to roto-translation couplings in layered structures (in which molecules tilt with respect to the planar normal) has yet to be rigorously examined by experiments. Another spin relaxation problem, which involves biaxial and/or chiral phases, certainly deserves a lot more attention both from the experimental and theoretical viewpoints.

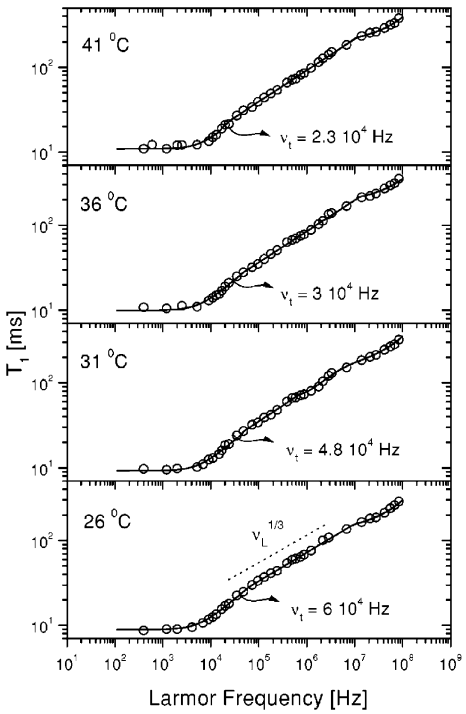

Fig. 12. Proton T_1 frequency dispersion curves for several temperatures in 3-PCH showing the decrease in the $T_1 \propto \nu^{1/2}$ power law (reproduced from Ref. [159] with the permission of the authors).

4.2. Proton studies

Proton NMR relaxometry of LCs, based on the conventional and field cycling experiments, deals with both intra- and inter-molecular contributions to the relaxation of proton spins. The lack of site specificity of tightly coupled protons in LCs is compensated by the advantages: (i) deuteration is not necessary, which often involves time-consuming and costly chemical syntheses, (ii) high proton signal-to-noise ratio, and (iii) the ability to study the translational SD. Thus, proton and deuteron spin relaxation studies are often complementary to each other in elucidating motional information in LCs. The interpretation of T_1 dispersion data over a limited frequency range can become problematic and should be viewed with care. In general, internal rotations within the LC molecule are assumed to be too fast to affect the proton spin relaxation, and the proton spin–lattice relaxation rate is often approximation by Eq.

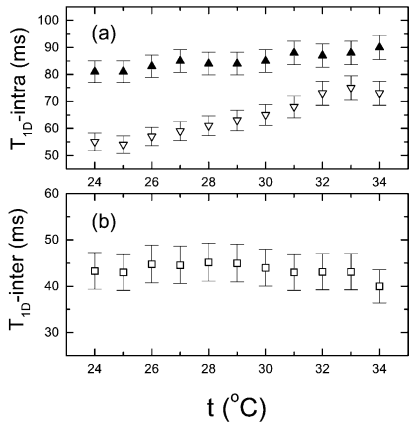

Fig. 13. (a) Intra-pair dipolar relaxation times in the nematic phase of 5CB-d_{11} (solid triangles) and 5CB (open triangles) versus the temperature at the external B field 0.41 T. (b) Inter-pair dipolar relaxation time versus the temperature in 5CB at $B = 0.34$ T [169].

(60) in which the cross-term contribution T_{1X} is set to zero.

The following observations can be made in a typical proton T_1 dispersion curve of LCs: the frequency behavior below 100 kHz is dominated by slow dynamics like ODF and above this frequency, MR and translational SD mechanisms become dominant in spin relaxation. Proton T_1 studies of N and SmA phases are fairly well understood [156]. A novel feature, the so-called quadrupolar dips [157], observed in proton T_1 dispersion curves of certain LCs is explained by cross relaxation of the proton system through fast relaxing ^{14}N quadrupolar nuclei. Recently, the spin relaxation in tilted smectic phases has attracted much attention. The SmC is a simple tilted phase. It is often argued that SmC phases are closer in structure to the N phase. Hence the T_1 frequency dependence (< 100 kHz) in SmC phases is ascribed to nematic-like ODF in some studies, while in others to layer undulations as seen in SmA phases. In a recent proton T_1 relaxometry study in the SmC phase of two LCs (8CB and HpAB) [158], there is a transition in the power law from a linear dependence to a square root one at a particular temperature, indicating both nematic-like ODF and layer undulations exist close to the SmC–N transition. The authors argued that pseudo nematic clusters may exist in the SmC phase. In a SmC phase, rotations of the molecular director (i.e. the long molecular axis) about the planar normal can occur without any distortion to the layers. Such slow motion is different from undulations (or two-dimensional director fluctuations) and has recently been shown to give a nematic-like ODF power law [106]. Indeed, assuming that these two motional mechanisms can be treated independently, the proton T_1 frequency dispersion in the bilayer SmC_2 phase of the LC 4-octylphenyl 2-chloro-4-(4-cyanobenzoloxy) benzoate (DB_8Cl) can be interpreted as shown in Fig. 11. It was found that the contribution of in-layer fluctuations of the molecular director (DF_N) exceeds that of the layer undulation over the entire studied frequency range. Another recent proton T_1 relaxometry study in the nematic phase of propylcyano-phenylcyclohexane (3-PCH) has shown [159] that the square root law ($T_1 \propto \omega^{\alpha}$, $\alpha = 1/2$) for ODF is sensitive to the temperature. Fig. 12 reproduces the T_1 data at four different temperatures. At 36 °C, the frequency dispersion has a transition from $\alpha = 1/2$ below $\nu_t = 30$ kHz to $\alpha = 0.37$ above 30 kHz. As seen in this figure, ν_t increases with decreasing temperature. Thus, the proton spin pairs experience reorientational fluctuations which are slow in comparison with ODF and that the molecular structure may play an important role for the observation of power law with $\alpha = 1/3$. For chiral molecules forming a SmC^* phase, it has been suggested [160] that an additional contribution is needed to account for slow modes arising from distortions of the helix. As mentioned before in connection with the roto-translation relaxation mechanism, the chiral compound $10FBTCO_1M_7$ exhibits a TGB_A phase and a SmC^* phase upon decreasing temperature [108]. It is interesting to compare the T_1 temperature profiles of the TGB_A–SmC^* transition with those of the SmA–SmC^* transition at different Larmor frequencies. The T_1 temperature profiles obtained at different Larmor frequencies show a continuous decrease of T_1 with decreasing temperature for the case of SmA–SmC^* transition. This is true for the TGB_A–SmC^* transition only for frequencies larger than 9 MHz. Below this frequency, the T_1 temperature profile shows increasing T_1 with decreasing temperature in the TGB_A phase, while the usual decreasing T_1 with decreasing temperature is obtained in the SmC^* phase. To explain the unusual temperature behavior in the TGB_A phase at Larmor frequencies lower than 9 MHz, roto-translation

couplings of molecules crossing the grain boundaries between adjacent blocks must be included for relaxing proton spins.

Proton T_1 relaxometry study has been carried out to investigate the lamellar (SmC) to columnar (ϕ_h) phase transition of a biforked mesogen [161]. By comparing the T_1 dispersion data in the SmC and ϕ_h phases, the structure of the ϕ_h phase can be inferred from the analysis of the molecular SD motion. The similarity of the T_1 dispersion curves in the intermediate Larmor frequency range suggests that at a local scale both phases are similar in their structures [162]. The hexagonal columnar phase, D_{ho}, formed by the discotic mesogen C_8HET [163,164] has also been studied by proton T_1 relaxometry. In the ϕ_h phase of bifork molecules, groups of these molecules play the role of discotic molecules in their stacking to form columns. However, the inter-columnar jump diffusion proposed for D_{ho} [102] can be ruled out in the ϕ_h phase as there is no plausible mechanism for a group of bifork molecules to diffuse together from one column to another one. Thus, the T_1 dispersion data at the intermediate frequency range are found to be quite different for the D_{ho} and ϕ_h phases. Incidentally, deuteron spin relaxation has recently been carried out to study rotational diffusions of discotic molecules in the D_{ho} phase of rufigallol [136], hexakis(*n*-hexyloxy)triphenylene (HAT6) [117] and fluorinated HAT6 [135]. These studies can also complement the works at the high Larmor frequency range of the proton T_1 dispersion curves.

Short range order fluctuations have recently been studied in the isotropic phase of a nematic [165] by measuring the T_2 dependence on the pulse interval (t) in the Carr–Purcell–Meiboom–Gill pulse sequence. Just above the clearing point (T_C), LC molecules can fluctuate in and out between locally ordered clusters and isotropic surroundings. The local magnetic field in clusters (H_a) is different from that of the isotropic surrounding (H_b). Using a model of two-site exchange, the observed T_2 vs t curves at different temperatures can be described by the Luz–Meiboom equation for exchange [166]. This allows the determination of the mean lifetime and modulation frequency $\delta\omega = \gamma(H_a - H_b)$ at different temperatures. Furthermore, the observation of $\delta\omega^2 \propto 1/(T - T^*)$ with $T^* = T_C - 1\,K$ seems to support the existence of short range order fluctuations in clusters of coherence length ξ.

The proton spin–lattice dipolar relaxation time (T_{1D}) is analogous to T_{1Q} of deuteron systems, and can be measured by the JB sequence. It is related to spectral densities given by Eq. (23) in the high temperature limit. While the proton T_{1Z} experiments of nematic LCs usually show appreciable temperature dependence at a particular Larmor frequency, the corresponding T_{1D} experiments show much less temperature dependence at the same frequency. Furthermore, T_{1D} frequency dispersion measurements show a clear $\nu^{1/2}$ dependence, indicating ODF is a predominant relaxation mechanism [167]. For a chain-deuterated 5CB (5CB-d_{11}), the phenyl proton pairs show pure intra-pair and inter-pair dipolar quasi-invariants. Both dipolar quasi-invariants relax independently to thermal equilibrium with the lattice. The T_{1D}-intra and T_{1D}-inter for the intra- and inter-pair quasi invariants can be measured by using different fixed delays (t_{12}) between the first two radio frequency pulses (e.g. $t_{12} = 30$ and 80 μs for the intra- and inter-pairs in 5CB, respectively) in the JB sequence [168,169]. Both T_{1D}-intra and T_{1D}-inter can provide information about different molecular fluctuations which cause the spin–lattice relaxation of each kind of quasi-invariant. Fig. 13 shows the temperature dependencies of T_{1D}-intra and T_{1D}-inter in the nematic phase of protonated 5CB and chain-deuterated 5CB-d_{11}. The weak temperature dependencies of T_{1D}-intra in 5CB-d_{11} and T_{1D}-inter in 5CB indicate that the predominant relaxation mechanism is ODF. In the nematic phase of 5CB, the temperature dependence of T_{1D}-intra reflects the motional behaviors due to both ODF and individual molecular motions. To check the possible contribution of intermolecular dipolar interactions to T_{1D}, the proton T_{1D}-intra was recently measured in the nematic phase of the methyl-deuterated *p*-azoxyanisole (PAA-d_6) in several dilution samples with perdeuterated PAA(PAA-d_{14}) at 27 MHz [170]. Since the results coincide for different isotope dilution samples, the intermolecular contribution to the relaxation of the intra-pair dipolar energy in PAA-d_6 is negligible. The observed temperature dependence of T_{1D} also confirms that ODF is the relevant relaxation mechanism for the dipolar reservoir, but its contribution according to Eq. (23) must be modified by a multiplicative factor

$\alpha = 1.46$ [170]. It remains to be seen how such a factor can be accounted for theoretically.

4.3. Carbon-13 studies

Here a brief survey of relaxation studies by ^{13}C NMR is given, mainly due to relatively few such studies in the recent past. To achieve high resolution ^{13}C spectra in LCs, one needs to employ high-power proton dipolar decoupling and perhaps also magic angle spinning (MAS) of the sample. The interpretation of ^{13}C spin–lattice relaxation is not as straightforward as deuteron relaxation, simply due to the fact that both dipolar interaction and chemical shift anisotropy must be taken into account. Indeed, at high magnetic fields the contribution from chemical shift anisotropy to ^{13}C relaxation is significant, especially for unprotonated carbons. Under MAS condition, the ^{13}C spectrum of LCs shows much sharper lines [171] and the contribution from chemical shift anisotropy to ^{13}C relaxation can be drastically reduced when the sample spinning rate is sufficiently high. Thus, the experimental requirements for ^{13}C spin relaxation study of LCs are quite demanding. However, interests in the dynamics of new materials, such as chiral smectogens showing FLC and/or AFLC phases, combining with recent advances in solid-state spectrometers have made the ^{13}C T_1 and linewidth measurements in LCs more popular. Here we will focus on two recent T_1 studies as examples: one is a chiral LC 4-(S)-2-methyloctanoyl) phenyl 4′-nonylbiphenyl-4-carboxylate(S-MONBIC) [171] and the other an antiferroelectric LC 4-(1-methylheptyloxycarbonyl) phenyl-4′-octyloxybiphenyl-4-carboxylate (S-MHPOBC) [172]. Both static and rotating samples under proton dipolar decoupling were used to study the SmA–SmC* transition in S-MONBIC. There is a marked line broadening of ^{13}C linewidths for the core carbons upon cooling into the SmC* phase in the static sample. This has been commonly observed in the chiral SmC phases, both by ^{13}C [173] and ^{2}H probes [143]. The ^{13}C line broadening may be caused by the chemical shift anisotropy which depends on the helicodal layer structure in the SmC* phase. Slow fluctuations of the molecular director (i.e. the long molecular axis) around the cone, the so-called Goldstone mode, do not affect the layer space, but may have an effect on the observed broadening of ^{13}C lines from the molecular core and tail. ^{13}C T_1 has been measured as a function of temperature in this sample under the MAS condition. There are definite jumps in T_1 values of the unprotonated carbons in S-MONBIC at the SmA–SmC* transition. Thus, the study has indicated a discontinuous change in the orientation and dynamics of the molecular core at the transition. In addition, a particular motional model was used to quantify the T_1 of protonated carbons in this chiral compound. Now S-MHPOBC exhibits an AFLC phase in which the molecules in the adjacent layers tilt in the oppose sense, i.e. SmC_A^*. ^{13}C T_1 measurements were carried in this sample under the MAS condition and with proton decoupling as a function of temperature. There is no jump in the ^{13}C T_1 for various carbon sites at the SmA–SmC_A^* phase transition [172]. Furthermore, the changes in the activation energies do not exist for the SmA and SmC_A^* phases for most of carbon sites except for the carbon nucleus at the chiral center, and the carbonyl carbon nuclei. This study seems to indicate that this AFLC does not show drastic changes in its dynamics at the SmA–SmC_A^* phase transition. Much more work is needed to clarify the motional behaviors at the tilted to non-tilted smectic phase transitions.

5. Relaxation in lyotropics

In this section, a very brief overview of recent relaxation studies will be given for lyotropic LCs and model bilayer systems using different nuclei. Halle and co-workers have used spin relaxation of quadrupolar nuclei (^{2}H, ^{23}Na, etc.) to obtain a wide range of properties for lyotropic LCs. Translational SD of surfactants or counterions over the interface can convey geometric and dynamic information relating to the microstructure of lyotropic LCs [174]. Nuclear spin relaxation due to director fluctuations in multilamellar fluid bilayer systems has been extensively considered by the Halle group [175]. These authors have taken couplings between the membranes in a multilamellar assembly into account to give a comprehensive description of the T_1 relaxation dispersion. This description differs from the predictions using the free membrane theory, in which couplings between individual membranes are

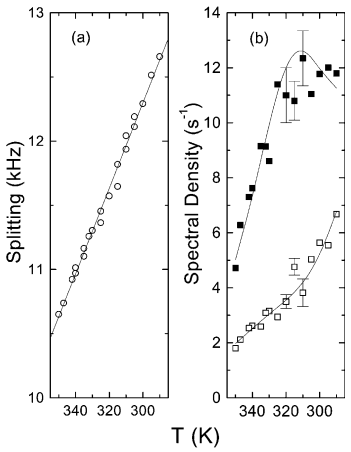

Fig. 14. (a) ^{14}N quadrupolar splitting versus the temperature. (b) Experimental spectral densities measured at 90° orientation (see text) versus the temperature. The solid curves are the calculated spectral densities based on a simple model of 'classical' aggregates [181].

neglected. Although both the free membrane and coupled membrane theories produce the same $1/\omega$ dispersion (see Eq. (37)) for lamellar phases, their ODF prefactors are, however, different. The lamellar phase is characterized by two elastic modulii: K_1 is associated with director splay (which is related to the membrane bending rigidity $\kappa = K_1 d$ where d is the bilayer period), and $\overline{B}$ is associated with longitudinal (along the optic axis) compression at a constant chemical potential [175]. Collective motions and bending rigidity have been studied by means of the proton T_1 frequency dependence in the multilamellar system of lipid and surfactant bilayers [176]. The relaxation mechanisms used to describe the T_1 dispersion curve over a wide frequency range of 10^2 to 10^8 Hz include layer undulations, translational diffusions, rotational diffusions and translational diffusion mediated reorientations (TR). The TR mechanism is included to account for the hindered diffusion of surfactants along curved lamellar surfaces. The nature of T_1 dispersion for TR depends on details of the molecular reorientation and the distribution of curvatures. For simplicity, by assuming local spherical curvatures Debye type TR spectral densities [177] were used. It was found that layer undulations dominated the low frequency T_1 dispersion in both unoriented and glass plate-oriented bilayer systems. The angular dependence of the T_1 dispersion for the oriented bilayer system provides a more critical analysis of the two-dimensional SD than in unoriented samples. The bending rigidity κ can be calculated for the studied bilayer systems at different levels of hydration. Furthermore, it is interesting to note that the derived κ values would be too large unless the coupled membrane theory of Halle is used to model the layer undulations.

A series of relaxation studies of vesicles and multilamellar dispersions of 1,2-dimyristoyl-sn-glycero-3-phosphocholine (DMPC) in the liquid crystalline state have been carried out by Brown and co-workers [68,69,89,96] using ^{2}H and ^{13}C. By means of temperature-, frequency- and orientation-dependent spin relaxation rates, these authors have demonstrated how a composite motional model may be used to extract the dynamics of lipid bilayers and biological membranes. For instance, collective motions are found less predominant in the case of DMPC/cholesterol than in pure DMPC, indicating an increased dynamical rigidity of lipid bilayers containing cholesterol [68,69]. It should be noted that Brown and co-workers have not taken the coupled membrane theory of layer undulations into consideration.

A proton NMR relaxometry study has recently been carried out on the micellar, hexagonal, cubic and lamellar phases of a lyotropic LC formed by the nonionic surfactant *n*-dodecylhexaoxyethylene glycol ($C_{12}E_6$) in water of various concentrations [178]. The proton T_1 dispersion curves are different in these phases, indicating that the relaxation behaviors are affected by motions associated with various local structures. At room temperature, the micellar phase is stable roughly below a 2% concentration of $C_{12}E_6$ and consists of long cylindrical rods dissolved in water. These rods show hexagonal symmetry just like those in the hexagonal phase. Upon decreasing the water content at room temperature, the system goes into a hexagonal phase, then a cubic phase followed by a lamellar phase. For this lyotropic, the structure of the lamellar phase depends on the water concentration. At higher water contents, the lamellar phase consists of planar regions that contain embedded cylinders, while those cylinders do not seem to exist in the lower water content lamellar phase. It was found that the relaxation in the lamellar phase is more complex than in the other phases. Besides fast MRs about the local axially symmetry axis, slightly slower

translational SDs, and slow motions like undulations, an additional relaxation contribution due to the exchange of $C_{12}E_6$ molecules between the planar and cylindrical regions must be used. The relaxation behaviors in the micellar and hexagonal phases of $C_{12}E_6$/water are quite similar, though there is a hint that the slow dynamics of lipid molecules shows different $T_1(\nu)$ power laws in these phases. The slow dynamics in the cubic phase is found to be nearly Lorentzian. This is rationalized by the fact that translational diffusions around the corners of a cubic lattice completely average out the intramolecular dipolar Hamiltonian.

The cubic (I_1) phase of the dodecyltrimethylammonium chloride (C_{12}TACl)/water has recently been studies by ^{2}H NMR relaxation of the α-deuteriated surfactant [179]. Models for the cubic phase suggest that a number of aggregates is arranged on a cubic lattice in a certain fashion. The remaining order of the surfactant at the aggregate site is found to be small (≈ 0.06) after surface diffusions and aggregate rotations. Deuteron T_{1Z} was measured as a function of the Larmor frequency (0.5–76.8 MHz) at different temperatures. All the T_{1Z} dispersion curves show a three-step character, and can be explained using the Lorentzian three-step model [180]. The results are discussed in relation to the prevailing structure models of the cubic phase. ^{14}N NMR can be used to study lyotropics when the large quadrupolar coupling has been motionally averaged to a reasonable value. Recently the methodology developed for ^{2}H relaxation in LCs has been applied to ^{14}N NMR study of the hexagonal phase of C_{12}TACl/D_2O [181]. The 70 wt% C_{12}TACl sample shows a typical Pake powder pattern with Δ being the quadrupolar splitting between the 90° edges. The ^{14}N spin–lattice relaxation times T_{1Z} and T_{1Q} were measured at 21.7 MHz using signals at the 90° edges to give spectral densities $J_1(\omega_0, 90°)$ and $J_2(2\omega_0, 90°)$. The temperature dependencies of Δ and spectral densities are reproduced in Fig. 14. A simple model of 'classical' aggregate [182], which uses fast local motions (described by J_f in a white spectrum) and slower surface SDs about the cylindrical aggregate axis, can explain the spin relaxation in this phase. The surface SD is described by an azimuthal correlation time τ_{az}, which can be related to the surface diffusion constant D_s and the radius of the cylindrical aggregate b by $\tau_{az} = b^2/4D_s$. The τ_{az} was found to be tens of nanoseconds and J_f increased from 1.1 to 6.5 s^{-1} upon decreasing temperature from 350 to 290 K.

Furó and co-workers have recently studied the counterion diffusion on an oppositely charged micellar surface in the micellar solutions of C_{16}TACl/D_2O [183] and C_{16}TABr/D_2O [184] by means of the field-dependent T_1 and T_2 measurements of quadrupolar nuclei. Both ^{35}Cl and ^{81}Br have $I = 3/2$ and large electric quadrupole moments. In general, $I = 3/2$ nuclei exhibit multiexponential transverse and longitudinal relaxation [185]. However, in these micellar solutions, the relaxation decays of ^{35}Cl and ^{81}Br are effectively exponential. These studies indicate the counterion surface diffusion coefficient is about 10^{-9} m^2/s, and the counterion diffuses much faster than the surfactant molecule so that these two entities cannot be closely associated on a time scale ≥ 100 ps.

Finally, the deuteron relaxation dispersion study has been carried out to examine of the surfactant aggregation behavior in aqueous solutions of decylammonium chloride (C_{10}ACl-αd_2, 5–29 wt%)/water [186]. The surfactant C_{10}ACl has a smaller headgroup in comparison with those used above. In the low concentration end (below the second critical micellar concentration (cmc), the micelles can be described as poly-disperse rather small aggregates, whose motions can be described as unhindered Brownian rotation. Above the second cmc, the micelles are rod shaped and grow with increasing surfactant concentration. As a consequence, the low frequency T_1 data seem to indicate that tumblings of rod shaped aggregates become restricted by their neighbors. The restricted reorientation of micelles is modeled using the slowly relaxing local structure model [100] for phases with no macroscopic order. The cage or tube formed by the neighbors of the aggregate prevents it from rotating through all angles of space with equal probability. The orientation of the tube defines the average orientation of the aggregate or director. The potential of mean torque is given by a double cone potential function with constant potential within the cone and infinitely hard wall at angles $\pm\beta$ and $\pm(\pi - \beta)$ relative to the director. This study concludes that at the studied concentrations the micelles are not wormlike, since the effective correlation time for the slowest processes increases with concentration, while the SD coefficient decreases with concentration.

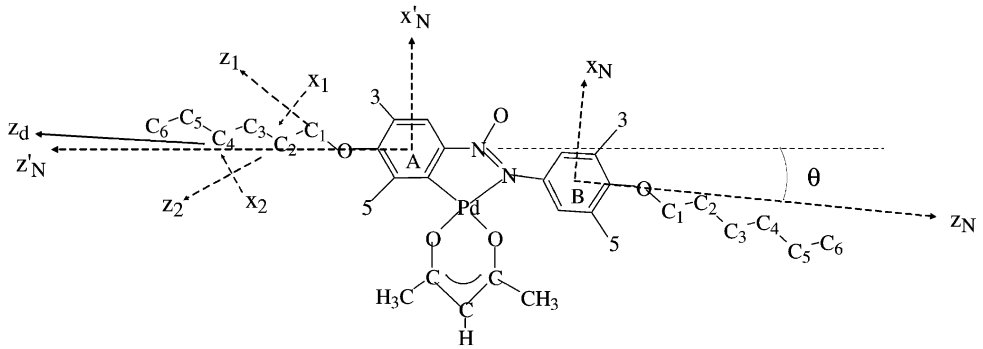

Fig. 15. Molecular structure of Azpac showing different coordinate systems. Sites 3 and 5 on rings A and B are deuterated in Azpac-d_4. The chains are deuterated in Azpac-d_{26}. The long molecular z_d axis makes a 1° angle with z'_N axis of (x'_N, y'_N, z'_N) frame which is fixed on ring A.

6. Other NMR studies: exotic phases

As mentioned above, the direction of average molecular tilt (θ_0) rotates in space as one goes from one smectic layer to another in a chiral SmC^* phase. On the other hand in the SmC^*_A phase, the average molecular tilt direction alternates between θ_0 and $-\theta_0$ as one goes from one smectic layer to the next while the azimuthal angle varies continuously to give a double helicodal structure. Deuteron NMR spectral patterns can provide direct microscopic evidence for the alternating tilt model of AFLCs [187]. Chiral molecules forming FLCs and AFLCs show a rich variety of chiral subphases, which have attracted much interest recently. Investigations of dynamics in FLCs and AFLCs by nuclear spin relaxation are still scarce. We have mentioned some such studies by ^{13}C NMR. There is NMR evidence that a chiral chain is motionally hindered in the liquid crystalline phase, as the chain is bent at the chiral center with respect to the molecular long axis [173,188–191]. The possibility of anomalous rotational dynamics has been hinted at by the deuteron T_{1Z} and T_{1Q} data in a partially ring-deuteriated chiral smectogen S-4-(methylbutyloxy)-carbonylphenyl 4-(10-undecenyloxy)-benzoate [192]. However, the indeterminacy of $D_\perp$ cannot be ruled out in this study. Another deuteron NMR study involves investigating order and dynamics in the chiral smectogen 8BEF5, partially deuterated in the chiral chain and the phenyl moiety [144,193]. Due to the relatively short chiral chain, the number of conformations is equal to 5. The AP method has been applied to model the quadrupolar splittings of all the deuterated sites in the SmA phase. The dynamics in the SmA phase of 8BEF5 has been described above.

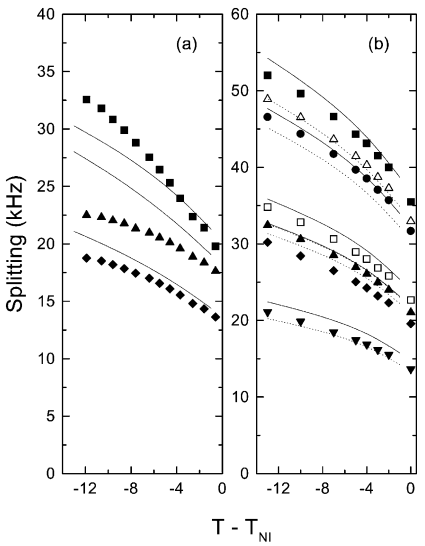

Fig. 16. Plots of quadrupolar splittings versus the temperature. (a) Azpac-d_4: squares, triangles and diamonds denote C^A_5, C^A_3 and $C^B_{3,5}$ ring data, respectively. Solid curves starting from the top are calculated values for C^A_5 and C^A_3, while the dashed curve is for $C^B_{3,5}$. (b) Azpac-d_{26}: closed squares, circles, uptriangles and down-triangles denote $C^{A,B}_1$, C^B_2, $C^A_3(C^B_4)$ and $C^{A,B}_5$, respectively. Open uptriangles, squares and diamonds denote C^A_2, C^A_4 and C^B_3, respectively. The calculated values are shown as either solid (chain A) or dashed (chain B) curves starting from the top for C^A_1, C^B_1, C^A_2, C^B_2, C^A_3, C^A_4, C^B_3, C^B_4, C^A_5 and C^B_5, respectively.

Even non-chiral polar molecules can form interesting tilted phases. For example, the DB_8Cl compound mentioned in Section 4.2 shows four mesophases upon decreasing temperature: N, bilayer SmA_2, bilayer SmC_2 and anticlinic-like ($SmC_?$) phases. In the SmC_2 phase, DB_8Cl molecules align

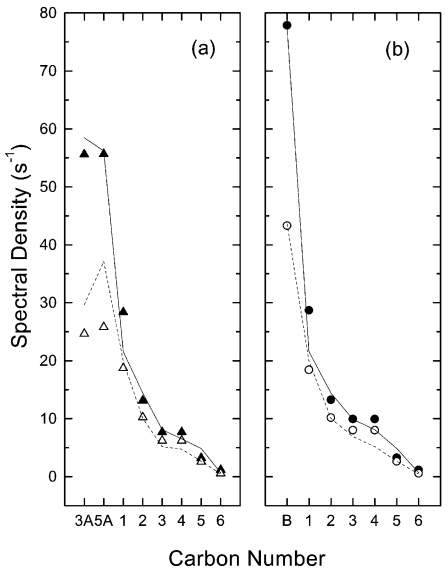

Fig. 17. Variation of the spectral densities $J_1(\omega)$ (closed symbols) and $J_2(2\omega)$ (open symbols) with the deuteron positions in the nematic pahse of Azpac at $T = 361.7$ K. (a) Data from chain A and ring A. (b) Data from chain B and ring B. Calculated spectral densities are shown as lines.

along the external magnetic field while the planar normal makes a tilt angle θ with respect to the B field. In the $SmC_?$ phase, an anticlinic arrangement is superimposed on the 'regular tilt', that is, one layer of molecules has an angle $\theta + \beta$ and the other layer has an angle $\theta - \beta$ with respect to the bilayer normal. β was found to be about 13° in this anticlinic phase [194]. Proton T_1 frequency dispersion and angular dependence have been studied in the $SmC_?$ phase. The measurements were explained by the same relaxation mechanisms as in the bilayer smectic C_2 phase. However, the translational diffusion was much slower in the low-temperature tilted phase and therefore dominated the relaxation rate over the whole frequency range. This observation seems to confirm indirectly the anticlinic molecular ordering in the $SmC_?$ phase.

Polymer dispersed liquid crystals (PDLC) consist of nematic LC droplets embedded in a polymer matrix. The confinement results in a large surface to volume ratio and may influence the molecular motions. There is a substantial number of NMR studies involving PDLCs and related systems. Here we highlight a proton relaxometry study of 5CB dispersed in an epoxy polymeric matrix [195]. The LC and the polymer represent a two-phase system. Both nematic droplets ($t = 26$ °C) and isotropic droplets ($t = 40$ °C) were studied over a broad Larmor frequency range (500 Hz–84 MHz). Two PDLC samples of different droplet sizes were used in the study. By comparing the droplet data, bulk 5CB data and the pure polymer data, the authors show that T_1 is dominated by the cross relaxation at the LC–polymer interface in the entire frequency range. Cross relaxation arises due to the polymer protons relaxing much faster (shorter T_1) than the bulk LC protons. Now the T_1 dispersion curve cannot be explained merely by adjusting the effective cross relaxation rate. In the low frequency range (< 1 MHz), an additional relaxation process is needed for both the nematic and isotropic droplets. For nematic droplets, the additional process is ascribed to reorientations mediated by translational displacement (RMTD or TR) suggested by Kimmich et al. [196]. For the isotropic droplets, the additional process is the exchange relaxation proposed by Edzes et al. [197]. The contribution of the exchange relaxation to T_1 is BPP-like [30]. The study also indicates that neither the square-root law for ODF at low frequencies in bulk LCs, nor the TR mechanism for diffusions along curved surfaces, dominates the low frequency relaxation behavior of 5CB in PDLCs.

Metallomesogens are metal containing LCs. They are not well studied, mainly due to their high transition temperatures, poor thermal stability and high viscosity. The acetylacetonate derivative of the cyclopalladated 4,4′-bis(hexyloxy)azoxybenzene (Azpac) is an exception, showing a nematic phase below 100 °C. Fig. 15 shows the molecular structure of Azpac whose molecular fragment formed by the Pd atom and the coordinated groups (the acetylacetonate ligand and the phenyl ring A) is planar and rigid, and whose dihedral angle between the planar fragment and the phenyl ring B is about 41°. The angle θ between the ring para axes is about 7°. Recently, deuterium NMR spectra were reported in the nematic phase of two isotopomers of Azpac: one deuterated in the positions 3 and 5 of both rings (Azpac-d_4) and the other deuterated in the hexyloxy chains (Azpac-d_{26}). In addition, deuteron T_{1Z} and T_{1Q} were also measured for these isotopomers [198,199]. The experimental quadrupolar splittings for Azpac-d_4 and Azpac-d_{26} are reproduced in Fig. 16(a) and (b), respectively. A

quantitative analysis of both quadrupolar splittings and the spectral densities was carried out for these isotopomers [200]. The quadrupolar splittings of sites 3 and 5 of ring B are identical, indicating fast phenyl ring flips. The AP method was used to model these quadrupolar splittings. In this study, each hexyloxy chain adopts 243 conformations. Only one chain is considered explicitly, since both chains are assumed identical in conformation for simplicity. To work out the potential of mean torque $U_{\text{ext}}(n, \Omega)$, the segmental interaction tensors from both chains are added in a common molecular frame (x_N, y_N, z_N). As seen in Fig. 15, chain A (identify as the hexyloxy chain attached to ring A) differs from chain B since there is an extra coordinate transformation for chain A (i.e. $(x'_N, y'_N, z'_N) \rightarrow (x_N, y_N, z_N)$). This geometric consideration accounts for the observed differences in the splittings and relaxation behaviors of the two chains. The calculated quadrupolar splittings are also plotted in Fig. 16. The spectral density data at 46 MHz were interpreted using the original decoupled model, viz. using jump constants k_1, k_2 and k_3. Fig. 17(a) and (b) show the site dependencies of spectral densities $J_1(\omega)$ and $J_2(2\omega)$ at $T = 361.7$ K for chain (ring) A and chain (ring) B, respectively. The theoretical predictions are also shown as lines in this figure. The derived rotational diffusion constants $D_{\|}$, $D_{\perp}$ and D_{R} (ring B) and internal jump constants (see Table 1) for Azpac can be found in Ref. [200].

Although we have not included in this review relaxation studies involving solutes dissolved in LCs, it is worthwhile to mention a recent study which makes use of an unusual solute (xenon-129) to study re-entrant nematics. ^{129}Xe NMR has been used to investigate dynamics in re-entrant nematic LC mixtures [201]. A comparison of the xenon T_1 and T_2 temperature dependencies acquired at 9.4 and 11.7 T has indicated that the relaxation of the dissolved xenon is dominated by modulations of the dipolar interaction between ^{124}Xe and ^{1}H. In particular, different activation energies found in SmA and N(RN) phases could be used to infer the xenon distribution among the packing of dimers in a 6OCB/8OCB mixture. The present study seems to suggest that ^{129}Xe is a viable technique for studying the dynamics, packing and evolution of re-entrant phenomenon in LCs.

7. Concluding remarks and outlook

LC research remains to be a vibrant field of study not only for the purpose of discovering new and fundamental physical phenomena, but also in the search for new industrial applications in different areas including LC displays, memory and detection devices. Moreover, new liquid crystalline materials are being generated at a rapid rate, whose chemical and physical properties must be thoroughly understood if possible applications are to be fully exploited. NMR spectroscopy has undoubtedly demonstrated among many other experimental techniques its usefulness in elucidating LC material properties such as phase structures, molecular ordering and organization, as well as individual and collective motional dynamics. The present review of NMR relaxation in LCs cannot be taken as an exhaustive search of the literature, and is written in the same spirit as my book [27] to provide the reader with some representative works that have appeared since the mid 1990s. Works not mentioned in this review are just as important, but have simply escaped the attention of this author. In any case, it is our hope that the review has provided a large variety of relaxation studies to indicate what has been done thus far to make NMR an important tool for extracting dynamical information from partially ordered systems: thermotropics, lyotropics and biomembranes. The present status of different theoretical models has been surveyed in order to show that the development of theories is important to allow the experimentalists to make progress. There are still many uncharted NMR territories both in theory and in experimentation, since new problems are posed by the discovery of new LC materials. For instance, there is still no clear understanding of nuclear spin relaxation in biaxial phases, in chiral materials, in non-chiral (banana) molecules showing ferroelectric and anti-ferroelectric properties, and in biologically ordered macromolecules. In addition, certain experimental difficulties exist to prevent the complete determination of site specific spectral density parameters. For example, deuteron NMR relaxation measurements cannot be performed in a chain-deuterated 10B1M7 sample below the SmA phase, since in

tilted smectic phases the doublet peaks become broad and overlapping for those deuterons residing near the top of the chain. The reason for the line broadening effects is not clear at present. It remains to be determined whether the effects are due to static or dynamic properties of the tilted smectic phases. However, the problem of line broadening in ^{13}C NMR of chiral materials has partially been overcome by combining high power proton decoupling and MAS. Perhaps the trick of using MAS can be applied to deuterium NMR studies of chiral molecules.

It would be useful to employ several different nuclei (e.g. ^{13}C, ^{1}H, ^{2}H) to study the same chiral mesogen and to interpret these relaxation data by the same set of model parameters in a self-consistent way. As demonstrated in several relaxation studies, it is useful to combine the orientational-, temperature- and frequency-dependent relaxation parameters in order to provide a better picture of molecular dynamics in LCs. With the increasing computer power at rapidly decreasing cost, computer simulation of experimental relaxation data becomes easier and possible for molecules with increasing molecular sizes.

In summary, we have reviewed relaxation and the dynamics of molecules in liquid crystalline phases. Both thermotropics and lyotropics have been considered. By and large, most studied phases are optically uniaxial. Relaxation in biaxial phases is still not well understood. The studied nuclei include ^{1}H, ^{2}H, ^{13}C, ^{14}N, ^{23}Na, ^{35}Cl, ^{79}Br and ^{129}Xe in the present review. We must point out that molecular dynamics can be studied by spin–lattice T_1 and spin–spin T_2 measurements, but sometimes this information may also come from spectral pattern simulations. The latter has been omitted in the present review. We believe that NMR relaxometry still has much to offer in the world of LC research and related fields such as proteins dissolved in bicelles.

Acknowledgments

We thank the Natural Sciences and Engineering Council of Canada for financial support. The technical support of N. Finlay is gratefully acknowledged.

References

[1] F. Reinitzer, Monatsh Chem. 9 (1888) 421.
[2] L. Onsager, Ann. NY Acad. Sci. 51 (1949) 627.
[3] W. Maier, A. Saupe, Z. Naturforsch. 13a (1958) 564.
[4] M.A. Cotter, J. Chem. Phys. 66 (1977) 1098.
[5] W.M. Gelbart, A. Gelbart, Mol. Phys. 23 (1977) 1387.
[6] G.H. Heilmeier, W. Helfrich, Appl. Phys. Lett. 13 (1968) 91.
[7] P.G. de Gennes, J. Prost, Physics of Liquid Crystals, Oxford University Press, Oxford, 1995.
[8] G. Vertogen, W.H. de Jeu, Thermotropic Liquid Crystals, Fundamentals, Springer, Berlin, 1988.
[9] S. Chandrasekhar, Liquid Crystals, Cambridge University Press, Cambridge, 1992.
[10] E.B. Priestley, P.J. Wojtowicz, P. Sheng (Eds.), Introduction to Liquid Crystals, Plenum Press, New York, 1974.
[11] G.R. Luckhurst, G.W. Gray (Eds.), The Molecular Physics of Liquid Crystals, Academic Press, London, 1979.
[12] J.W. Doane, J.J. Visintainer, Phys. Rev. Lett. 23 (1969) 1421.
[13] M. Weger, B. Cabane, J. Phys. Colloq. 30 (1969) C4-72.
[14] R. Blinc, D.L. Hogenbloom, D.E. O'Reilly, E.M. Peterson, Phys. Rev. Lett. 23 (1969) 969.
[15] C.E. Tarr, M.A. Nickerson, C.W. Smith, Appl. Phys. Lett. 17 (1970) 318.
[16] R.Y. Dong, C.F. Schwerdtfeger, Solid State Commun. 9 (1970) 707.
[17] M.F. Brown, J. Chem. Phys. 77 (1982) 1576.
[18] C.G. Wade, Ann. Rev. Phys. Chem. 28 (1977) 47.
[19] R.R. Vold, in: J.W. Emsley (Ed.), Nuclear Magnetic Resonance of Liquid Crystals, Reidel, Dordrecht, 1985, p. 253.
[20] R. Blinc, M. Luzar, M. Mali, R. Osredkar, J. Seliger, M. Vilfan, J. Phys. Colloq. 37 (1976) C3-73.
[21] F. Noack, Prog. NMR Spectrosc. 18 (1986) 171.
[22] A.G. Redfield, Adv. Magn. Reson. 1 (1965) 1.
[23] C. Polnaszek, G.V. Bruno, J.H. Freed, J. Chem. Phys. 58 (1973) 3185.
[24] D. Frezzato, G. Kothe, G.J. Moro, J. Phys. Chem. B 105 (2001) 1281.
[25] A. Abragam, The Principles of Nuclear Magnetism, Clarendon Press, Oxford, 1961.
[26] J.W. Emsley (Eds.), Nuclear Magnetic Resonance of Liquid Crystals, Reidel, Dordrecht, 1985.
[27] R.Y. Dong, Nuclear Magnetic Resonance of Liquid Crystals, Second ed., Springer, New York, 1994.
[28] G.R. Luckhurst, C.A. Veracini (Eds.), The Molecular Dynamics of Liquid Crystals, Kluwer, Dordrecht, 1994.
[29] E.E. Burnell, C. de Lange (Eds.), NMR of Orientationally Ordered Liquids, Kluwer, Dordrecht, 2002.
[30] N. Bloembergen, E.M. Purcell, R.V. Pound, Phys. Rev. 73 (1948) 679.
[31] R.K. Wangsness, F. Bloch, Phys. Rev. 89 (1953) 278.
[32] I. Solomon, Phys. Rev. 99 (1955) 559.
[33] F. Bloch, Phys. Rev. 102 (1956) 104.
[34] F. Bloch, Phys. Rev. 105 (1957) 1206.
[35] K. Tomita, Prog. Theor. Phys. 19 (1958) 541.
[36] R. Kubo, K. Tomita, J. Phys. Soc. Jpn 9 (1954) 888.

[37] H.W. Spiess, in: P. Diehl, E. Fluck, R. Kosfeld (Eds.), NMR Basic Principles and Progress, vol. 15, Springer, Heidelberg, 1978, p. 55.
[38] M. Goldman, J. Magn. Reson. 149 (2001) 160.
[39] R.Y. Dong, in: J.C. Lindon (Ed.), Encyclo. Spectroscopy and Spectrometry, Academic Press, New York, 1999, p. 1568.
[40] J. Jeener, P. Broekaert, Phys. Rev. 157 (1967) 232.
[41] S. Wimperis, G. Bodenhausen, Chem. Phys. Lett. 132 (1986) 194.
[42] S. Wimperis, J. Magn. Reson. 83 (1989) 509.
[43] H. Bildsøe, J.P. Jacobsen, K. Schaumberg, J. Magn. Reson. 23 (1976) 137.
[44] J.P. Jacobsen, H. Bildsøe, K. Schaumberg, J. Magn. Reson. 23 (1976) 153.
[45] S.B. Ahmad, K.J. Packer, J.M. Ramsden, Mol. Phys. 33 (1977) 857.
[46] O. Mensio, R.C. Zamar, D.J. Pusiol, S. Becker, J. Chem. Phys. 110 (1999) 8155.
[47] O. Mensio, C.E. González, R.C. Zamar, J. Chem. Phys. 116 (2002) 1530.
[48] J. Jeener, A. Vlassenbroek, P. Broekaert, J. Chem. Phys. 103 (1995) 1309.
[49] S. Gustafsson, B. Halle, Mol. Phys. 80 (1993) 549.
[50] R.Y. Dong, Liq. Cryst. 16 (1994) 1101.
[51] E. Berggren, R. Tarroni, C. Zannoni, J. Chem. Phys. 99 (1993) 6180.
[52] E. Berggren, C. Zannoni, Mol. Phys. 85 (1995) 299.
[53] P.L. Nordio, P. Busolin, J. Chem. Phys. 55 (1971) 5485.
[54] P.L. Nordio, U. Segre, in: G.R. Luckhurst, G.W. Gray (Eds.), The Molecular Physics of Liquid Crystals, Academic Press, New York, 1979, p. 411.
[55] J.M. Bernassau, E.P. Black, D.M. Grant, J. Chem. Phys. 79 (1982) 253.
[56] R.R. Vold, R.L. Vold, J. Chem. Phys. 88 (1988) 1443.
[57] R. Tarroni, C. Zannoni, J. Chem. Phys. 95 (1991) 4550.
[58] T.P. Trouard, T.M. Alam, M.F. Brown, J. Chem. Phys. 101 (1994) 5229.
[59] G.J. Moro, P.L. Nordio, J. Chem. Phys. 89 (1985) 997.
[60] A. Brognara, P. Pasini, C. Zannoni, J. Chem. Phys. 112 (2000) 4836.
[61] H.C. Torrey, Phys. Rev. 92 (1953) 962.
[62] H.C. Torrey, Phys. Rev. 96 (1954) 690.
[63] H.A. Resing, H.C. Torrey, Phys. Rev. 131 (1963) 1102.
[64] G.J. Krüger, Z. Naturforsch. Teil A 24 (1969) 560.
[65] S. Žumer, M. Vilfan, Phys. Rev. A 17 (1978) 424.
[66] M. Vilfan, S. Žumer, Phys. Rev. A 21 (1980) 672.
[67] S. Žumer, M. Vilfan, Phys. Rev. A 28 (1983) 3070.
[68] T.P. Trouard, T.M. Alam, J. Zajicek, M.F. Brown, Chem. Phys. Lett. 189 (1992) 67.
[69] T.P. Trouard, A.A. Nevzorov, T.M. Alam, C. Job, J. Zajicek, M.F. Brown, J. Chem. Phys. 110 (1999) 8802.
[70] P.A. Beckmann, J.W. Emsley, G.R. Luckhurst, D.L. Turner, Mol. Phys. 54 (1986) 97.
[71] R.Y. Dong, G.M. Richards, Chem. Phys. Lett. 171 (1990) 389.
[72] R.Y. Dong, Phys. Rev. A 43 (1991) 4310.
[73] A. Ferrarini, G.J. Moro, P.L. Nordio, Liq. Cryst. 8 (1990) 593.
[74] R.Y. Dong, J. Lewis, E. Tomchuk, E. Bock, J. Chem. Phys. 69 (1978) 5314.
[75] T.M. Barbara, R.R. Vold, R.L. Vold, J. Chem. Phys. 79 (1983) 6338.
[76] T.M. Barbara, R.R. Vold, R.L. Vold, M.E. Neubert, J. Chem. Phys. 82 (1985) 1612.
[77] D. Goldfarb, R.Y. Dong, Z. Luz, H. Zimmermann, Mol. Phys. 54 (1985) 1185.
[78] J.S. Lewis, E. Tomchuk, H.M. Hutton, E. Bock, J. Chem. Phys. 78 (1983) 632.
[79] J.S. Lewis, J. Peeling, E. Tomchuk, W. Danchura, J. Bozek, H.M. Hutton, E. Bock, Mol. Cryst. Liq. Cryst. 144 (1987) 57.
[80] P.J. Flory, Statistical Mechanics of Chain Molecules, Interscience, New York, 1969.
[81] R. Blinc, M. Luzar, M. Vilfan, M. Burgar, J. Chem. Phys. 63 (1975) 3445.
[82] J.A. Marqusee, M. Warner, K.A. Dill, J. Chem. Phys. 81 (1984) 6404.
[83] P. Pincus, Solid State Commun. 7 (1969) 415.
[84] R.L. Vold, R.R. Vold, M. Warner, J. Chem. Soc. Faraday Trans. II 84 (1988) 997.
[85] W. Wölfel, F. Noack, M. Stohrer, Z. Naturforsch. 30a (1975) 437.
[86] G. Van der Zwan, L. Plomp, Liq. Cryst. 4 (1989) 133.
[87] E.A. Joghems, G. Van der Zwan, J. Phys. II 6 (1996) 845.
[88] R.Y. Dong, X. Shen, J. Phys. Chem. A 101 (1997) 4673.
[89] A.A. Nevzorov, M.F. Brown, J. Chem. Phys. 107 (1997) 10288.
[90] R.Y. Dong, J. Lewis, E. Tomchuk, E. Bock, J. Chem. Phys. 69 (1978) 5314.
[91] G.D. Williams, J.M. Beach, S.W. Dodd, M.F. Brown, J. Am. Chem. Soc. 107 (1985) 6868.
[92] E. Lindahl, E. Edholm, J. Chem. Phys. 115 (2001) 4938.
[93] A. Szabo, J. Chem. Phys. 81 (1984) 150.
[94] P. Ukleja, J. Pirš, J.W. Doane, Phys. Rev. 14 (1976) 414.
[95] J.H. Freed, J. Chem. Phys. 66 (1977) 4183.
[96] A.A. Nevzorov, T.P. Trouard, M.F. Brown, Phys. Rev. E 58 (1998) 2259.
[97] R.Y. Dong, Mol. Cryst. Liq. Cryst. 141 (1986) 349.
[98] D.E. Woessner, J. Chem. Phys. 36 (1962) 1.
[99] C.F. Polnaszek, G.V. Bruno, J.H. Freed, J. Chem. Phys. 58 (1973) 3185.
[100] C.F. Polnaszek, J.H. Freed, J. Phys. Chem. 79 (1975) 2283.
[101] G. Lipari, A. Szabo, J. Am. Chem. Soc. 104 (1982) 4546.
[102] S. Žumer, M. Vilfan, Mol. Cryst. Liq. Cryst. 70 (1981) 39.
[103] R. Blinc, M. Burgar, M. Luzar, J. Pirš, I. Zupančič, S. Žumer, Phys. Rev. Lett. 33 (1974) 1192.
[104] J.F. Harmon, B.H. Muller, Phys. Rev. 182 (1969) 400.
[105] K.H. Schweikert, F. Noack, Z. Naturforsch. Teil A 44 (1989) 597.
[106] A. Carvalho, P.J. Sebastião, A.C. Ribeiro, H.T. Nguyen, M. Vilfan, J. Chem. Phys. 115 (2001) 10484.
[107] S. Renn, T. Lubensky, Phys. Rev. A 38 (1998) 2132.
[108] J.L. Figueirinhas, A. Ferraz, A.C. Ribeiro, H.T. Nguyen, F. Noack, J. Phys. II France 7 (1997) 79.

[109] S. Marcelja, J. Chem. Phys. 60 (1974) 3599.
[110] J.W. Emsley, G.R. Luckhurst, C.P. Stockley, Proc. R. Soc. Lond. Ser. A 381 (1982) 117.
[111] J. Struppe, F. Noack, Liq. Cryst. 20 (1996) 595.
[112] R.Y. Dong, G.M. Richards, J. Chem. Soc. Faraday Trans. 88 (1992) 1885.
[113] R.Y. Dong, L. Friesen, G.M. Richards, Mol. Phys. 81 (1994) 10117.
[114] R.Y. Dong, Mol. Phys. 88 (1996) 979.
[115] L. Calucci, M. Geppi, C.A. Veracini, R.Y. Dong, Chem. Phys. Lett. 296 (1998) 357.
[116] X. Shen, R.Y. Dong, J. Chem. Phys. 108 (1998) 9177.
[117] X. Shen, R.Y. Dong, N. Boden, R.J. Bushby, P.S. Martin, A. Wood, J. Chem. Phys. 108 (1998) 4324.
[118] R.Y. Dong, Phys. Rev. E 60 (1999) 5631.
[119] R.Y. Dong, A. Carvalho, P.J. Sebastião, H.T. Nguyen, Phys. Rev. E 62 (2000) 3679.
[120] R.Y. Dong, M. Cheng, J. Chem. Phys. 113 (2000) 3466.
[121] R.Y. Dong, C.R. Morcombe, L. Calucci, M. Geppi, C.A. Veracini, Phys. Rev. E 61 (2000) 3466.
[122] R.Y. Dong, Phys. Rev. E 57 (1998) 4316.
[123] R.Y. Dong, G.M. Richards, Mol. Cryst. Liq. Cryst. Sci. Technol., Sect. A 262 (1995) 339.
[124] E. Helfand, J. Chem. Phys. 54 (1971) 4651.
[125] E. Helfand, E.R. Wasserman, T.A. Weber, Macromolecules 13 (1980) 526.
[126] J. Skolnick, E. Helfand, J. Chem. Phys. 72 (1980) 5489.
[127] R.Y. Dong, Chem. Phys. Lett. 329 (2000) 92.
[128] R.Y. Dong, J. Chem. Phys. 114 (2001) 5897.
[129] G.R. Luckhurst, C. Zannoni, P.L. Nordio, U. Segre, Mol. Phys. 30 (1975) 1345.
[130] B.J. Gertner, K. Lindenberg, J. Chem. Phys. 94 (1991) 5143.
[131] R.Y. Dong, in: E.E. Burnell, C.A. de Lange (Eds.), NMR of Orientationally Ordered Liquids, Kluwer, Dordrecht, 2002.
[132] R.Y. Dong, L. Chiezzi, C.A. Veracini, Phys. Rev. E 65 (2002) 041716.
[133] A.V. Zakharov, A.V. Komolkin, A. Maliniak, Phys. Rev. E 59 (1999) 6802.
[134] A.V. Zakharov, R.Y. Dong, Phys. Rev. E 63 (2000) 011704.
[135] R.Y. Dong, N. Boden, R.J. Bushby, P.S. Martin, Mol. Phys. 97 (1999) 1165.
[136] R.Y. Dong, C.R. Morcombe, Liq. Cryst. 27 (2000) 897.
[137] V. Rutar, M. Vilfan, R. Blinc, E. Bock, Mol. Phys. 35 (1978) 721.
[138] J.M. Goetz, G.L. Hoatson, R.L. Vold, J. Chem. Phys. 97 (1992) 1306.
[139] P.J. Sebastião, A.C. Ribeiro, H.T. Nguyen, F. Noack, Z. Naturforsch. A: Phys. Sci. 48 (1993) 851.
[140] P.J. Sebastião, A.C. Ribeiro, H.T. Nguyen, F. Noack, J. Phys. II 5 (1995) 1707.
[141] R.Y. Dong, Chem. Phys. Lett. 251 (1996) 387.
[142] D. Catalano, M. Cifelli, M. Geppi, C.A. Veracini, J. Phys. Chem. A 105 (2001) 34.
[143] D. Catalano, M. Cavazza, L. Chiezzi, M. Geppi, C.A. Veracini, Liq. Cryst. 27 (2000) 621.
[144] L. Chiezzi, V. Domenici, M. Geppi, C.A. Veracini, R.Y. Dong, Chem. Phys. Lett. 358 (2002) 257.
[145] A. Yoshizawa, A. Yokoyama, H. Kikuzaki, T. Hirai, Liq. Cryst. 14 (1993) 53.
[146] L. Calucci, M. Geppi, J. Chem. Inf. Comput. Sci. 41 (2001) 1006.
[147] D. Catalano, C. Forte, C.A. Veracini, J.W. Emsley, G.N. Shilstone, Liq. Cryst. 2 (1987) 345.
[148] D. Catalano, M. Geppi, C.A. Veracini, C. Forte, Mol. Cryst. Liq. Cryst. 221 (1992) 7.
[149] M. Cifelli, C. Forte, M. Geppi, C.A. Veracini, Mol. Cryst. Liq. Cryst. 372 (2001) 81.
[150] R.Y. Dong, G.S. Bates, X. Shen, Mol. Cryst. Liq. Cryst. 331 (1999) 143.
[151] M. Vilfan, N. Vrbančič-Kopač, P. Ziherl, G.P. Crawford, Appl. Magn. Reson. 17 (1999) 329.
[152] M. Vilfan, T. Apih, A. Gregorovič, B. Zalar, G. Lahajnar, S. Žumer, G. Hinzec, R. Böhmer, G. Althoff, Magn. Reson. Imaging 19 (2001) 433.
[153] S.A. Rozanski, R. Stannarius, H. Groothues, F. Kremer, Liq. Cryst. 20 (1996) 59.
[154] N.J. Heaton, G. Kothe, J. Chem. Phys. 108 (1998) 8199.
[155] M. Geppi, S. Pizzanelli, C.A. Veracini, Chem. Phys. Lett. 343 (2001) 513.
[156] F. Noack, K.H. Schweikert, in: G.R. Luckhurst, C.A. Veracini (Eds.), The Molecular Dynamics of Liquid Crystals, Kluwer, Dordrecht, 1994, p. 233.
[157] R. Kimmich, Tomography, Diffusometry, Relaxometry, Springer, Berlin, 1998.
[158] A. Acosta, D. Pusiol, Phys. Rev. E 60 (1999) 1808.
[159] R.H. Acosta, D.J. Pusiol, Phys. Rev. E 63 (2000) 011707.
[160] A. Ferraz, A.C. Ribeiro, H.T. Nguyen, Mol. Cryst. Liq. Cryst. 331 (1999) 67.
[161] C. Cruz, J.L. Figueirinhas, P.J. Sebastião, A.C. Ribeiro, F. Noack, H.T. Nguyen, B. Heinrich, D. Guillon, Z. Naturforsch. 51a (1996) 155.
[162] A.C. Ribeiro, P.J. Sebastião, C. Cruz, Mol. Cryst. Liq. Cryst. 362 (2001) 289.
[163] C. Cruz, A.C. Ribeiro, Mol. Cryst. Liq. Cryst. 331 (1999) 75.
[164] C. Cruz, P.J. Sebastião, J. Figueirinhas, A.C. Ribeiro, H.T. Nguyen, C. Destrade, F. Noack, Z. Naturforsch. 53a (1998) 823.
[165] E.R. Gasilova, V.A. Shevelev, S.Ya. Frenkel, Liq. Cryst. 27 (2000) 573.
[166] Z. Luz, S.J. Meiboom, J. Chem. Phys. 39 (1963) 1587.
[167] O. Mensio, R.C. Zamar, D.J. Pusiol, S. Becker, J. Chem. Phys. 110 (1999) 8155.
[168] H. Schmiedel, S. Grande, B. Hillner, Phys. Lett. 91A (1982) 365.
[169] O. Mensio, C.E. Gonzàlez, D.J. Pusiol, R.C. Zamar, R.Y. Dong, Physica (2002) in press.
[170] O. Mensio, R.C. Zamar, F. Casanova, D.J. Pusiol, R.Y. Dong, Chem. Phys. Lett. 358 (2002) 457.
[171] A. Yoshizawa, H. Kikuzaki, M. Fukumasa, Liq. Cryst. 18 (1995) 351.
[172] K. Tokumaru, B. Jin, S. Yoshida, Y. Takanishi, K. Ishikawa, H. Takezoe, A. Fukuda, T. Nakai, S. Miyajima, Jpn J. Appl. Phys. 38 (1999) 147.
[173] S. Yoshida, B. Jin, Y. Takanishi, K. Tokumaru, K. Ishikawa,

H. Takezoe, A. Fukuda, T. Kusumoto, T. Nakai, S. Miyajima, J. Phys. Soc. Jpn 68 (1999) 9.
[174] B. Halle, P.-O. Quist, I. Furó, Liq. Cryst. 14 (1993) 227.
[175] S. Gustafsson, B. Halle, J. Chem. Phys. 106 (1997) 9337.
[176] J. Struppe, F. Noack, C. Klose, Z. Naturforsch. 52a (1997) 681.
[177] S. Žumer, M. Vilfan, J. Phys. 46 (1985) 1763.
[178] E.E. Burnell, D. Capitani, C. Casieri, A.L. Segre, J. Phys. Chem. B 104 (2000) 8782.
[179] M. Törnblom, R. Sitnikov, U. Henriksson, Liq. Cryst. 7 (2000) 943.
[180] H. Nery, O. Söderman, D. Canet, H. Walderhaug, B. Lindman, Journal 88 (1984) 1655.
[181] R.Y. Dong, Mol. Phys. 99 (2001) 637.
[182] P.-O. Quist, B. Halle, I. Furó, J. Chem. Phys. 95 (1991) 6945.
[183] N. Hedin, I. Furó, P.O. Eriksson, J. Phys. Chem. B 104 (2000) 8544.
[184] N. Hedin, I. Furó, J. Phys. Chem. B 103 (1999) 9640.
[185] L.G. Werbelow, in: D.M. Grant, R.K. Harris (Eds.), Encyclopedia of Nuclear Magnetic Resonance, vol. 6, Wiley, Chichester, 1997, p. 4092.
[186] M. Törnblom, R. Sitnikov, U. Henriksson, J. Phys. Chem. B 104 (2000) 1529.
[187] B. Zalar, A. Gregorovič, M. Simsič, A. Zidanšek, R. Blinc, Phys. Rev. Lett. 80 (1998) 4458.
[188] T. Nakai, S. Miyajma, Y. Takanishi, S. Yoshida, A. Fukuda, J. Chem. Phys. B 103 (1999) 406.
[189] K. Miyachi, Y. Takanishi, K. Ishikawa, H. Takezoe, A. Fukuda, Phys. Rev. E 55 (1997) 1632.
[190] Y. Ouchi, Y. Yoshioka, H. Ishii, K. Seki, M. Kitamura, R. Noyori, Y. Takanishi, I. Nishiyama, J. Mater. Chem. 5 (1995) 2297.
[191] B. Jin, Z. Ling, Y. Takanishi, K. Ishikawa, H. Takezoe, A. Fukuda, M. Kakimoto, T. Kitazume, Phys. Rev. E 53 (1996) R4295.
[192] R.Y. Dong, M. Cheng, K. Fodor-Csorba, C.A. Veracini, Liq. Cryst. 27 (2000) 1039.
[193] D. Catalano, L. Chiezzi, V. Domenici, M. Geppi, C.A. Veracini, R.Y. Dong, K. Fodor-Csorba, Macromol. Chem. Phys. (2002) in press.
[194] A. Carvalho, P. Sebastião, A. Ferraz, A. Ribeiro, H. Nguyen, Eur. Phys. J. E 2 (2000) 351.
[195] D. Schwarze-Haller, F. Noack, M. Vilfan, G.P. Crawford, J. Chem. Phys. 105 (1996) 4823.
[196] R. Kimmich, S. Stapf, J. Niess, J. Appl. Phys. 75 (1994) 529.
[197] H.T. Edzes, E.T. Samulski, J. Magn. Reson. 31 (1978) 207.
[198] L. Calucci, D. Catalano, M. Ghedini, N.L. Jones, D. Pucci, C.A. Veracini, Mol. Cryst. Liq. Cryst. Sci. Technol., Sect. A 290 (1996) 87.
[199] L. Calucci, C. Forte, M. Geppi, C.A. Veracini, Z. Naturforsch. A Phys. Sci. 53 (1998) 427.
[200] R.Y. Dong, C.R. Morcombe, L. Calucci, M. Geppi, C.A. Veracini, Phys. Rev. E 61 (2000) 1559.
[201] J. Bharatam, C.R. Bowers, J. Phys. Chem. B 103 (1999) 2510.